Ocean acidification responses in paralarval squid swimming behavior using a novel 3D tracking system

Citation: Zakroff, Casey, et al. "Ocean Acidification Responses in Paralarval Squid Swimming Behavior Using a Novel 3D Tracking System." Hydrobiologia, vol. 808, no. 1, Feb. 2018, pp. 83–106.

As Published: http://dx.doi.org/10.1007/s10750-017-3342-9

Publisher: Springer International Publishing

Persistent URL: http://hdl.handle.net/1721.1/114393

Version: Author's final manuscript: final author's manuscript post peer review, without publisher's formatting or copy editing

Ocean Acidification Responses in Paralarval Squid Swimming Behavior Using a Novel 3D Tracking System

Casey Zakroff[1,2,3], T. Aran Mooney[2], Colin Wirth[2]

Corresponding Author: Casey Zakroff, czakroff@whoi.edu, ORCID: 0000-0001-6979-1857

[1]Massachusetts Institute of Technology-Woods Hole Oceanographic Institution Joint Program in Oceanography/Applied Ocean Science and Engineering, Cambridge, MA, USA

[2]Biology Department, Woods Hole Oceanographic Institution, Woods Hole, MA, USA

[3]Red Sea Research Center, King Abdullah University of Science and Technology, Thuwal, 23955-6900, Saudi Arabia

Keywords: hypercapnia, cephalopod, larvae, movement analysis, stress physiology

Acknowledgments

We thank D. Remsen, the MBL Marine Resources Center staff, and MBL *Gemma* crew for their support in acquiring squid. R. Galat and the facilities staff of the WHOI ESL provided system support. D. McCorkle, KYK Chan, and M. White provided valuable insight on the OA system. E. Moberg, A. Beet, and A. Solow assisted in the development and coding of the 3D model system. We also thank E. Bonk, K. Hoering, M. Lee, D. Weiler, and A. Schlunk for their assistance and input with the experiments. This material is based upon work supported by the National Science Foundation Graduate Research Fellowship under Grant No. 1122374. This project is funded by NSF Grant No. 1220034.

Abstract

Chronic embryonic exposure to ocean acidification (OA) has been shown to degrade the aragonitic statolith of paralarval squid, *Doryteuthis pealeii*, a key structure for their swimming behavior. This study examined if day-of-hatching paralarval *D. pealeii* from eggs reared under chronic OA demonstrated measurable impairments to swimming activity and control. This required the development of a novel, cost-effective, and robust method for 3D motion tracking and analysis. Squid eggs were reared in pCO_2 levels in a dose-dependent manner ranging from 400 - 2200 ppm. Initial 2D experiments showed paralarvae in higher acidification environments spent more time at depth. In 3D experiments, velocity, particularly positive and negative vertical velocities, significantly decreased from 400 to 1000 ppm pCO_2, but showed non-significant decreases at higher concentrations. Activity and horizontal velocity decreased linearly with increasing pCO_2, indicating a subtle impact to paralarval energetics. Patterns may have been obscured by notable individual variability in the paralarvae. Responses were also seen to vary between trials on cohort or potentially annual scales. Overall, paralarval swimming appeared resilient to OA, with effects being slight. The newly developed 3D tracking system provides a powerful and accessible method for future studies to explore similar questions in the larvae of aquatic taxa.

Introduction

Ocean acidification (OA) has emerged as a prominent threat to marine systems, with rising atmospheric CO_2 concentrations decreasing ocean pH at rates unparalleled in geologic history (Doney et al., 2009; Honisch et al., 2012). Coastal systems are particularly susceptible due to freshwater influx and concurrent anthropogenic impacts, e.g. eutrophication, reducing the buffering capacity and increasing the pH variability of these waters (Gledhill et al., 2015). Nearshore marine systems provide nursery habitat to a range of ecological and economically vital species, including the longfin inshore squid, *Doryteuthis pealeii*, a keystone species in the Northwest Atlantic coastal trophic web and a substantial fishery (Macy III, 1982; Beck et al., 2001; Jacobson, 2005; Hunsicker & Essington, 2008). This member of the demersal Lolignid squids is a seasonal migrator, overwintering on the continental shelf and breeding nearshore south of the Mid-Atlantic Bight, before coming north and inshore to areas like Vineyard Sound, MA, USA from late spring through early autumn for peak breeding season (Macy III & Brodziak, 2001; Jacobson, 2005). The squid leave mops of egg capsules tied to the seafloor, each containing embryos, 50 - 200 per capsule, which must develop under whatever conditions they are laid in, enduring environmental stress until hatching (Arnold et al., 1974; Jacobson, 2005). At hatching, the paralarvae must cope both with the shock of the transition into a neritic, planktonic phase and the continued stress of their environment until they are transported by prevailing currents (Robin et al., 2014). Paralarval survivorship is naturally low, with greatest mortality occurring during the no net growth, post-hatch period while transitioning from yolk reserves to exogenous feeding (Vidal et al., 2002a; Robin et al., 2014). Sublethal physiological changes to embryonic condition, metabolism, or sensory systems imposed by environmental stressors, such as OA, could express as shifts in hatchling paralarval swimming activity and behavior. Any

impairments arising during this sensitive transitional phase could be detrimental not only to individual squid success, but also to overall population structure (Byrne, 2011; Robin et al., 2014).

Swimming is key to paralarval squid survival; the mantle fins are rudimentary post-hatch, therefore hatchlings rely primarily on jetting for motion, which is necessary in capturing prey and avoiding predators (Vecchione, 1981). Paralarvae operate at intermediate Reynolds numbers (25 - 90), balancing between the viscous world at low speeds and a more inertial world during their high speed jets (Bartol et al., 2009a). They are also negatively buoyant: slowly, passively sinking before jetting upwards in bursts, displaying a characteristic 'hop and sink' pattern, which is believed to conserve energy (Haury & Weihs, 1976; Staaf et al., 2014). Jetting is an energetically costly means of motion, but one that provides remarkable propulsive efficiency at the paralarval stage (Bartol et al., 2008, 2009b). During the post-hatch transitional phase, paralarvae must operate with a finite fuel reserve, the yolk, to power their jets as they avoid predation and learn to predate, but this same energy source is also tapped to mitigate stress and maintain homeostasis (Vidal et al., 2002a; Sokolova et al., 2012).

Under natural conditions, the fluid surrounding the chorions of *D. pealeii* embryos within an egg capsule reaches dramatically low pH (7.34) and oxygen concentrations (1.9 μmol l^{-1}) prior to hatching: a potentially taxing physiological state that may be exacerbated by ocean acidification (Long et al., 2016). Both hypercapnia and decreased pH can elicit metabolic depression in marine ectotherms, a common stress coping response (Guppy & Withers, 1999; Sokolova, 2013). Depression of oxygen consumption rate has been shown to occur in the embryos and hatchling paralarvae of high-CO_2 exposed eggs of the European squid, *Loligo vulgaris* (Rosa et al., 2014). Cephalopods have substantial homeostatic machinery, energy-

dependent acid-base transporters, with which they can maintain extracellular pH (Gutowska et al., 2010). They may be capable, then, of reallocating energy across active biological processes, in order to retain their overall metabolic rate (Sokolova et al., 2012). Reduced dorsal mantle length (DML) and increased embryonic development time have been seen in *D. pealeii* hatchlings exposed to chronic OA, which may be indicative of such a homeostatic response (Kaplan et al., 2013). Both metabolic depression and energy budget reallocation during embryonic development could result in a subsequent reduction in hatchling paralarvae swimming activity or speed.

The statoliths (small aragonitic stones connected to sensory hair cells) are the core sensory structures for control of motion balance, and orientation in the cephalopods (Messenger, 1970; Arkhipkin & Bizikov, 2000). Absence of the paralarval statolith resulting from a lack of strontium in artificial seawater has been shown to cause aberrant "spinning" behaviors in several cephalopod taxa (Hanlon et al., 1989). *D. pealeii* paralarvae have demonstrated a reduction in statolith size and quality after exposure to high levels of CO_2 during development (Kaplan et al., 2013). This present study sought to repeat and expand on the above mentioned study by recording and tracking the movement of squid paralarvae in order to examine if chronic embryonic exposure to OA caused impairments to their general swimming activity and orientation ability.

Squid paralarvae present a distinct challenge in larval tracking with current methodologies. As small (approximate DML of 1.8 mm, total length of 3 mm), translucent organisms, squid paralarvae are well-suited to digital particle image velocimetry (DPIV) studies (Bartol et al., 2008, 2009a, 2009b). These studies, while advantageous for dissecting the mechanics of motion and flow in many taxa, are primarily done in two-dimensions (2D) as the

set up and equipment, and subsequent costs associated with requiring both a laser and high-speed camera, are substantial (Stamhuis & Videler, 1995; Fuchs et al., 2004; Wheeler et al., 2013).

Early techniques of larval videography and tracking were enacted in simple, cost-effective 2D systems, such as petri dishes or round aquariums, where the animal was recorded in the horizontal *x*, *y* plane from a camera directly above (Wassersug & von Seckendorf Hoff, 1985; Villanueva et al., 1997; Budick & O'Malley, 2000). These systems were limiting for a study with squid paralarvae given the dominance of vertical motions in their swimming behavior (Staaf et al., 2014). Stereoscopic camera systems are commonly used in the field to detect accurate depth and positional information of oceanic organisms (Klimley & Brown, 1983; Boisclair, 1992). In lab, this method requires lighting from the front, however, which can alter the behavior of positively phototactic organisms like squid.

Using two perpendicular cameras allows for unbiased lighting while still capturing the organism in all three dimensions. Such methods can produce a clear movement track, but often require specially designed systems, either with motorized camera set ups or with uniquely shaped aquaria that limit movement range in the *y* axis (Coughlin et al., 1992; Cachat et al., 2011a, 2011b). We found we were limited by existing tracking software being both prohibitively expensive and, in testing, proving not to successfully function in tracking videos of the squid paralarvae. In order to observe swimming at the resolution and accuracy needed to examine our OA-driven questions, we had a clear need to develop a method of three-dimensional (3D) analysis that would not limit or coerce the motion of the organism and would produce clear, well-lit video wherein the organism could be tracked effectively by readily available software.

The aim of this study was to evaluate the potential effects of ocean acidification on post-hatch paralarval squid, *D. pealeii*, swimming behavior using newly-hatched paralarvae reared

under a range of CO_2 concentrations (and thus a range of pH treatments). Across their range, and dependent on season, adult *D. pealeii* can be found in depths ranging from 1 - 400 m, temperatures ranging from 4 - 28 ºC, and salinities ranging from 30-37 ppt. Juvenile and adult *D. pealeii* have been found in the Hudson-Raritan estuary, a system with much greater temperature, salinity, and pH variation than the coastal shelf, which may indicate these life stages are capable of at least acute exposure to a wide range of environmental conditions (Jacobson, 2005). Comprehensive measurements of in situ environmental pH in *D.* pealeii habitat across its range have not been performed to our knowledge, but ranges of mean shelf $pH_{total}(20)$ of 7.85 - 8.05 and $fCO_2(20)$ of 400 - 700 ppm were reported from North Carolina to New Hampshire from a coastal carbon cruise conducted in summer (July/August) (Wang et al., 2013). Little is documented about the ecology or environmental exposures of the paralarval life phase of squid, but rearing experiments with Loliginids indicate high water quality and a recommended pH > 8.0 are best for their survival (Hanlon et al., 1983; Vidal et al., 2002b).

Our study focused on specimens from and comparisons to the Vineyard Sound, MA system where *D. pealeii* eggs are laid every summer. This work encompassed a range of CO_2 levels between current ambient (400 ppm) and the elevated treatment used in Kaplan et al. (2013). The high treatment, 2200 ppm, is predicted for 2300 based on IPCC IS92a, but is naturally found in the very extreme inshore estuary conditions of Vineyard sound (Caldeira & Wickett, 2003; McCorkle et al., 2012). The intent was to examine the physiological scope and sensitivity of hatchling paralarval swimming. We hypothesized, based on initial work by Kaplan et al. (2013), that activity levels, speed, and control of orientation would be impaired in OA-exposed paralarvae due to impairments to their physiological and sensory systems. The question posed required a robust visualization of the energetics and kinematics of paralarval swimming,

which required the development of a novel, simple, and feasible method of 3D paralarval tracking and analysis that we present here alongside the experimental data.

Materials and Methods

Squid Collection and Husbandry

Experiments were conducted at the Environmental Systems Laboratory (ESL) at the Woods Hole Oceanographic Institution, Woods Hole, MA, USA from June-August 2013, May-October 2014, and May-June 2015. This timing corresponds with the peak breeding season of the Atlantic Longfin squid, *Doryteuthis pealeii*, in the nearshore of New England (Jacobson, 2005). Although the full breadth and physical properties of *D. pealeii* egg habitat is not well described, eggs in New England waters are typically found at depths less than 50 m, with temperature and salinity ranges of 10 - 23 ºC, and 30 - 32 ppt, respectively (McMahon & Summers, 1971; Jacobson, 2005; Shashar & Hanlon, 2013). Squid were collected during trawls in Vineyard Sound at 10-30 meters depth by the Marine Biological Laboratory (MBL). Sea surface temperatures in Vineyard Sound, MA, USA ranged from 8.4 - 25.8 ºC with a mean of 19.4 ºC from May - October (compiled for 2013 - 2015 from NOAA Station BZBM3). Bottle samples (n = 5) were taken in Vineyard Sound at 20 m depth (processed for Alk/DIC using VINDTA) in the morning once every two weeks from late July - late September 2014 off of the MBL squid trawler at the site of capture, along with accompanying CTD casts (CastAway CTD, SonTek, San Diego, USA). These data show a temperature range of 17.4 - 19.6 ºC, salinity range of 31.3-32.5 psu, total alkalinity range of 2148.1 - 2195.2 µmol / kg, DIC range of 1962.7 - 2038.2 µmol / kg, pH_{total} range of 7.96 - 8.00, and pCO_2 range of 439.9 - 486.5 ppm, but are limited in scope in reference to the whole breeding season.

Intact, adult squid (mid-sized, 20-25 cm DML without fin tears/skin lesions) were hand-selected from the trawl catch at the MBL's Marine Resources Center dock. Individuals were gently placed in seawater-filled coolers and transported by car to the ESL immediately after the ship's return (< 6 hours post-capture), and transferred to the ESL holding aquaria. All transport activity was performed as carefully and expediently as possible to minimize stress to the breeding adults, but overall capture and transit stress was unavoidable. Eighteen squid were selected for breeding; reproductively active females (differentiated by their bright orange accessory nidamental gland) and males, displaying visible and dense sperm packets, were selected in a 2:1 female:male ratio to enhance breeding probability.

Upon arrival at the ESL, squid were split equally between two holding tanks (120 cm diameter, 70 cm depth), maintaining the 2:1 gender ratio. Holding tanks were flow-through, using water pumped directly from Vineyard Sound (approximately 100 yards offshore of the ESL) that had been sand-filtered and cooled to 15°C (Salinity = 33 psu, pH_{nbs} = 7.96), and continuously bubbled with air. This temperature was within the range naturally experienced by the adults during the breeding season and reduced thermal and metabolic stress on the adults, as well as the incidence of infighting and cannibalism, compared to if they were housed at ambient temperatures. Squid were fed once per day with locally captured killifish, *Fundulus heteroclitus*, gathered from Salt Pond, Woods Hole, MA. Upon discovery, mops of egg capsules were transferred into a bucket of water from the adult tank and carried to the room containing the ocean acidification system where they were hand sorted into the experimental cups. Only good quality egg capsules, those that were long and finger-like with an orange tinge and laid in neat mops, were chosen; egg capsules contained between 90 - 300 eggs, which is expected for this

species (Arnold et al., 1974; Maxwell & Hanlon, 2000). Adult squid were maintained in the tanks at the ESL until they died following breeding.

Ocean Acidification System

In brief, for each trial, *D. pealeii* egg capsules collected from the squid aquaria were randomly sorted into flow-through cups (1-liter PET food service containers [Solo Foodservice, Lake Forest, IL]) filled with seawater delivered via drip lines from upstream equilibration chambers. These chambers were bubbled with CO_2 and air to maintain respective CO_2 concentrations (ranging from 400 ppm to 2200 ppm). All rearing cups were contained within a 20ºC water bath under a 14:10 hour light:dark cycle. No temperature acclimation was conducted for the eggs, as this level of temperature shift did not appear to notably impact embryonic development or survival, or paralarval viability. This temperature and light regime approximated the average values in Vineyard Sound (19.4 ºC) across the breeding season, late April to early October. A rearing temperature of 20 ºC was chosen as it reflected natural conditions, to replicate the conditions in the previous work by Kaplan et al. (2013), and because temperature controls the development time of *D. pealeii*, and so resulted in a consistent 14 day time to hatching at the control pCO_2 (McMahon & Summers, 1971; Zeidberg et al., 2011). There were three cups containing two egg capsules each and one chemical control cup per treatment per trial. Flow rates to the cups were approximately 20 l day^{-1}, which prevented waste accumulation. Water quality of the experimental cups was monitored using a pH probe (Orion Star™ A329, Thermo Fisher Scientific Inc., Waltham, MA, USA) every three days, while alkalinity, salinity, and spectrometric pH readings were taken weekly in order to calculate pCO_2 with CO2SYS (Table 1)

(a full OA system description, experimental procedure, and CO_2 monitoring methods can be found in the Electronic Supplementary Material).

Paralarvae Sampling

Squid embryos were allowed to develop undisturbed in the OA system. Upon hatching, paralarvae from each cup were subsampled for a range of experiments, including behavioral videography. At the end of each hatching day, all paralarvae were removed from the system and preserved (anesthetized with 7.5 % w/v $MgCl_2$ mixed with equal part seawater and preserved in 70% ethanol) ensuring that all hatchlings used were less than 24 hours old. Over the first 3 - 6 days of hatching, 10 - 20 individual paralarvae per cup per treatment were collected for behavioral videos, in order to obtain multiple analyzable videos per treatment per trial. Paralarvae were haphazardly selected from the cups, avoiding those that exhibited a constant spinning behavior, which has been described both as an aberrant effect of aquarium-rearing and as a potential stereotyped predator defense (Hanlon et al., 1989; York & Bartol, 2016). Tests in 2013 demonstrated there was no difference in this behavior across CO_2 treatments (ANOVA, $F_{5, 21} = 2.31$, $p = 0.0805$). As there was only one arena/camera set up, videography was done for one experimental cup at a time. Per each cup, the arena was filled with water from the control cup for that treatment. Individual paralarvae (n = 10 - 15) from the experimental cup were transferred using a plastic pipet and kept within a 24 well plate (Falcon® Brand 2.0 cm^2 well area, 3.5 mL well volume, Corning Inc., Corning, NY, USA) filled with water from the same cup, one paralarva per well, until filming occurred. A filming period for one cup took at most an hour ([1 minute acclimation + 2 minutes recording + 1 minute removal and reset] * 10 - 15 paralarvae = 40 - 60 minutes per cup). It was assumed, although not tested, that water quality in the well plate

and arena was that of the experimental treatment sampled and did not notably change over the brief filming period. The arena and well plate were refilled for each filming period and treatments were selected from in a rotation, so as to not bias sampling by time of day. Overall more videos were recorded than were analyzed in both the 2D and 3D systems for all analyses, as only videos where the paralarvae was visible, away from the corners, exhibiting normal swimming/responses, and, in the case of the 3D metrics, trackable could be used (Table 1)

Swimming Behavior Experiments

Over the course of developing a viable 3D system, two different arenas were used resulting in two separate swimming behavior experiments. Experiment 1 consisted of Trials 1, 2 and 4 of 2013 and Trial 1 of 2014 (Table 1). Trials were run in a tall, rectangular arena that constrained movement in the *y* axis, but only 2D vertical swimming data could be tracked and analyzed from this system. Implemented in Experiment 2 (Trials 2, 3, and 4 in 2014 and in Trial 1 of 2015; Table 1), the cubic arena and model system allowed for full 3D tracking and analysis.

Wall effects were considered for both experiments, however the viscous effects of walls at low Reynolds numbers should not impact paralarvae given their size and speed (Vogel, 1981). Damage caused by wall impacts is a common source of mortality among aquarium housed squid, and it is best to make the walls visible to help avoid this, however this would have obscured recording and lighting (Summers et al., 1974). Many paralarvae interacted with the walls during recordings, but this did not appear to cause harm or behavioral shifts, although paralarvae were not subsequently checked for dermal abrasions. Increasing the available swimming volume from the 2D to the 3D arena was intended to reduce potential arena effects, although overall arena size was limited by available space (e.g. camera viewing scope within the covered light box).

In order to determine acclimation time, 10-minute recordings of individual paralarvae (9 useable videos analyzed of 20 videos taken), sampled from all treatments, placed into the arena were conducted. Paralarval activity, described by jetting or active mantle pulsation, showed no significant differences across 1-minute bins of the ten-minute observation period (Kruskal-Wallis, $p = 0.9284$). We do not claim that the paralarvae became accustomed to the arena, however there were no significant changes to their behavior within a reasonable recording timeframe (Supplementary Materials, Fig. S1). An acclimation time of 1 minute was therefore used for both experiments, in order to maximize the sample size of videos taken (Table 1).

Experiment 1: 2D Swimming Behavior

The trials of the first experiment took place during the summer of 2013 and in May of 2014. Experiment 1 used a preliminary 2D filming arena constructed from 500 mL tissue culture flasks (Corning Inc., Corning, NY, USA) by removing the top, capped portion, creating a standing container with internal dimensions of 10.6 cm width, 3.2 cm depth, and 14.0 cm height (*x*, *y*, and *z* axes) (Fig. S2a). All plastic containers were soaked for 24 hours in seawater and DI-water rinsed prior to use. Black card stock was attached to the back of the arena for contrast between the translucent organism and the background, allowing for better paralarval tracking. 400 mL of water from the corresponding CO_2 level was added to the chamber, corresponding to a 10.5 cm x 3.2 cm x 11.4 cm (*x*, *y*, and *z*) volume. This provided a large area, compared to the organism's size (approximately 3 mm), in the *x* and *z* axes while constraining movement in the *y* axis. This chamber was placed within a photobox (76.2 cm^3, B&H Foto & Electronics Corp, NY), which was covered with black tarp to block ambient light. Two LED panels with diffuser plates were placed on either side of the chamber to create equal lighting from both directions.

The strong photopositive response by paralarvae required lights be placed precisely and set to equal intensities to exclude directional bias. Two HD video cameras were placed inside the photobox at a 90º angle to the experimental chamber, one above (Sony HDR-XR550V) fastened to a wooden frame and one in front (Sony HDR-CX 580V). Only information from the front camera was used in later analyses due to poor larval visibility for tracking in footage from the top-mounted camera. Videos were recorded at 29.97 frames per second.

For each video, an individual paralarva was pipetted from the tray directly into the center of the chamber. After the one-minute acclimation period, swimming behavior was recorded for one minute. Paralarvae were removed from the chamber using a pipet and were anesthetized with 7.5 % w/v $MgCl_2$ mixed with equal part seawater before being preserved in 70% ethanol.

Experiment 1 Data Analysis

Individual paralarvae videos were tracked using Tracker, marking the eyes of the paralarvae, which were the most distinct and trackable feature (Open Source Physics, comPADRE Digital Library). Variability in the 2D system's video quality, due to issues of light reflection and clarity, and individual paralarval trackability (many paralarvae stayed near the walls, entrained in the meniscus, or expressed the aforementioned spinning behaviors, which made videos unusable) resulted in uneven sampling amongst the 2D data (total n = 394, Table 1). Organisms were tracked using the autotracker function when video quality allowed this for capability, but this function was corrected with manual tracking as needed. Positional data (*x* & *z* coordinates) were produced for each frame within the 60-second interval, totaling 1799 points per recording. The *z* axis of the arena was divided into equal thirds of 4.73 cm and positional data were sorted into these depth bins for the top, middle, and bottom of the container using

Excel (Excel for Mac 2011, Microsoft Corp., Redmond, WA, USA). The number of frames per bin, directly proportional to time spent in each depth section, was calculated for each individual and compared across CO_2 treatment groups.

Experiment 2: 3D Swimming Behavior

The trials of the primary experiment using the developed 3D analysis system took place in the summer of 2014 and May of 2015. The recording arena for the 3D filming consisted of the bottom portion of a plastic display box (10.2 cm x 10.2 cm x 18.4 cm, Amac Plastic Products Corp., Petaluma, CA, USA) (Fig. S2b). Black card stock was attached to the back of the container in the *x, z* plane and black cotton cloth laid on the bottom of the container in the *x, y* plane, again to contrast translucent paralarvae. In the 2D arena, excessive light reflection could obscure paralarvae near the walls and a strong meniscus could entrain paralarvae to the surficial corners, but the greater area, and increased wall clarity of the 3D arena prevented these issues.

The 3D filming arena was set up in the same manner as the 2D arena within the photobox. The camera lenses were each aligned to the centroid of the chamber for their respective viewing planes (Fig. 1, A & B). Each camera was connected to its own monitor outside of the photobox so that paralarval swimming could be observed during the trials.

The chamber bottom measured 92.16 cm^2 inside (9.6 cm x 9.6 cm); therefore, the chamber was filled to 9.6 cm depth with water of the appropriate CO_2 concentration to create an 884.7 cm^3 cube to contain the organism (the model system requires a cubic water volume, as outlined below, but the size can be changed). Individual paralarvae were pipetted from a holding tray directly into the center of the filming arena and allowed to acclimate for one minute. Swimming behavior was then recorded for two minutes; increased from the previous 2D

experiments due to the improved video quality and tracking output of the 3D system as well as the need for more path data for the more complex 3D metrics. The two minute period was concluded by flashing a laser pointer into the filming chamber, which provided a synchronization point for the top and side videos. Paralarvae were then removed from the chamber, anesthetized, and preserved in 70% ethanol.

Experiment 2 Data Analysis

Videos from the top and side cameras were synched using the laser flash and cut to two-minute clips for each paralarva. Videos were tracked using Tracker, using the eyes of the paralarvae as the tracking feature, as with the 2D experiment. Although the 3D arena did not diminish video quality as the 2D arena did, a large number of videos could still not be used, due to paralarvae staying at walls and corners, or spinning (total tracked video n = 157, Table 1). Positional data were produced for each frame in both viewing planes, resulting in 3,598 points for each recording plane (x, z) and (x, y). Tracker functioned with the origin point for the calibrating axes being set based on the orientation of the camera. Thus prior to correction for 3D, the positional data were all transformed into the same 0, 0, 0 axes frame set at the bottom left corner of the front plane of the filming arena using Excel.

To merge the two separate 2D positional datasets into a 3D dataset, the filming arena was modeled as two series of diminishing planes, "side" and "top" (Fig. 1, C & D). In any given video frame, the front plane of the chamber had the true dimensions of the arena, 92.16 cm^2. Along the axis perpendicular to the axes of the video frame, the planes diminish in the image due to the vanishing point effect, up unto the back of the arena. The value of the length of the side of the cube was known (Q = 9.6 cm). The organism was in some plane along the perpendicular axis,

so its position within its plane in the image is proportional to its true position in a 9.6 cm-sided square, such that

1) $$\frac{Q_s}{Q} = \frac{x_{is}}{x}$$

2) $$\frac{Q_s}{Q} = \frac{z_{is}}{z}$$

3) $$\frac{Q_t}{Q} = \frac{x_{it}}{x}$$

4) $$\frac{Q_t}{Q} = \frac{y_{it}}{y}$$

where Q_s and Q_t are the lengths of the plane the organism is in within the image and x_{is}, z_{is}, x_{it} and y_{it} are the positional coordinates of the organism within that plane, in the side and top, respectively.

The positional values of the organism were measureable within the coordinate axes of the front plane using Tracker: x_s and z_s for the side, and x_t and y_t for the top. The positional values of the organism in its image plane were modeled as the difference between these measured coordinates and the side of the right triangle formed between the front plane and the organism's image plane (Fig. 1, C & D):

5) $$x_{is} = x_s - q_{is}/\sqrt{2}$$

6) $$z_{is} = z_s - q_{is}/\sqrt{2}$$

7) $$x_{it} = x_t - q_{it}/\sqrt{2}$$

8) $$y_{it} = y_t - q_{it}/\sqrt{2}$$

where q_{is} and q_{it} are the hypotenuse of the right triangles for the side and top, respectively. The hypotenuse divided by the square root of two provides a measure of distance between the front

plane and the organism's image plane. It follows then that Q_s and Q_t are different to Q by twice this measure:

9) $$Q_s = Q - 2 * \left(q_{is}/\sqrt{2}\right)$$

10) $$Q_t = Q - 2 * \left(q_{it}/\sqrt{2}\right)$$

The length of the side of the backmost plane was measureable within the film image for both the side and top camera (q_{bs} and q_{bt}, respectively). The ratios between these values and the length of the filming arena are equal to the ratios between the distances between planes, q_{is} and q_{it}, and the true distance of the image plane along the perpendicular axis, y and z, respectively:

11) $$\frac{q_{bs}}{Q} = \frac{q_{is}}{y}$$

12) $$\frac{q_{bt}}{Q} = \frac{q_{it}}{z}$$

This results in an over-constrained system. Datasets for individual paralarva with all measured values were run through a MATLAB (R2016b, MathWorks, Inc., Natick, MA, USA) custom-built script (in the Electronic Supplementary Material and at https://github.com/czakroff/3D-Swimming-Behavior) which calculated the *x*, *y*, and *z* values for the system by using least sum of squares to determine the values for each frame that result in the least error. These data were then run in a separate MATLAB custom-built script (in the Electronic Supplementary Material and at https://github.com/czakroff/3D-Swimming-Behavior) to visualize paralarval swimming tracks and calculate a range of 3D metrics, including total distance traveled (cm), 3D velocity (cm s^{-1}), vertical and horizontal velocities (cm s^{-1}), and volume (cm^3) transited for each individual paralarva. All video measurements were taken and all subsequent analyses using the model system and codes were run using centimeters. However, all results have been shifted into millimeters for better readability in publication. 3D metrics were

further analyzed in ten-second time bins across the 120-second recording period for each individual paralarvae, to examine individual variability and assess if paralarvae across treatments retained consistent overall behavior patterns while in the 3D arena.

Since squid paralarvae swim in a characteristic cycle of vertical jetting and sinking, average vertical velocity canceled out to zero. Therefore, vertical velocity was subdivided into average positive vertical velocity, representative of upward jets, and negative vertical velocity, representative of sinking and uncommon, but possible, downward jets. Average jet velocity was calculated by measuring the magnitude of the peaks, above a threshold of 0.5 cm s^{-1} (based on visual assessment of the data and on a reported range of jetting velocities in Bartol et al., 2009a), of the 3D velocity data across the two-minute recording period for each paralarvae. Jetting rate was likewise calculated by enumerating these velocity peaks for each paralarvae.

Turning angles for each paralarva's path were calculated between sequential motion vectors in the *x*, *y* plane at a resolution of thirty frames of video, or approximately one second of motion. Tortuosity, a metric of path convolution defined as the ratio of the length of an animal's path to the distance between the start and end points of that path, was calculated for each paralarva on path segments of thirty frames of video continuously along the entire path (Benoit-Bird & Gilly, 2012). The one-second resolution for these metrics was chosen to analyze individual paralarval paths on a reasonable temporal scale and reduce small-scale motion noise.

While thresholds of video quality and organism visibility limited the total number of videos useable in the 3D tracking analysis, many more videos were useable for simpler analyses. In some cases the side video was trackable or could be visually assessed while the top was not, so a random subset (n = 282, Table 1) of 3D videos taken was analyzed for time spent in depth bins, as in the 2D experiment. A separate randomly selected subset of approximately ten of the two-

minute paralarva swimming videos taken was analyzed per treatment per trial (n = 167, Table 1) for general ethography. Sections of each video were coded as either active, defined as a paralarvae jetting or pulsing its mantle, or inactive, defined as sinking, non-motile, and non-pulsing. Two observers each independently coded the same subset of 10 individual paralarvae to establish consistency in the definitions and then separately coded different subsets of the full dataset. Ethographic observations of activity were compiled as percent time active (converted from number of frames using the video frame rate) for the entire two-minute recording period for each individual paralarva.

Statistics

Statistical analyses were run in MATLAB, Python (3.5.2), and Excel. Normality was tested for using the Shapiro-Wilk test ($\alpha = 0.05$) and by examining quantile plots of the data for each factor, both within each treatment and as a whole. Datasets that were normally distributed were tested for differences among CO_2 treatments with a single factor ANOVA, while nonparametric data were tested with Kruskal-Wallis (KW) tests. Any significant ($p < 0.05$) KW test was subsequently run through a Dunn's posthoc test to determine which groups were significantly different from each other. Linear trend lines of the medians for each factor across CO_2 treatments were plotted in order to examine goodness of fit to the trend. Variability was examined through calculation of the variance, comparable within a metric, and the coefficient of variation (CV), which is comparable across metrics. All normally distributed statistics are reported as means ± 1 standard deviation (SD) while nonparametric statistics are reported as medians and interquartile range (IQR).

Results

Water Quality

No significant differences (Kruskal-Wallis, $p > 0.05$ for pH_{total} and pCO_2 for all trials) in water quality were seen between experimental cups within a treatment, so values are compiled and reported by treatment (Table 1). Temperature and salinity were stable across the duration of a trial, but varied slightly between trials, most likely due to local environmental variability. pCO_2 equilibrations were harder to control at higher concentrations, likely due to variability in the alkalinity and flow rate of ESL water (potentially due the expanded system, longer time frame, and increased demand in 2014 & 2015), as input gas concentrations and pressure were maintained throughout experiments and pH_{total} remained consistent within trials (Table 1). Results are grouped and reported by input gas concentration for concision, but it should be noted that the 2200 ppm group encompasses a range from 1750 - 2400 ppm in calculated pCO_2 values.

Experiment 1: 2D Depth

Squid paralarvae showed a slight, but significant (KW, $p < 0.001$) difference in proportion of time spent in the top depth bin between CO_2 treatment groups in 2013 (Fig. 2A), but no significant response in 2014 (KW, $p = 0.078$)(Fig. 2B). In the compiled dataset, within the top depth bin, the 400 and 1300 ppm CO_2 treatment groups were found to be different from the 1900 and 2200 ppm treatment groups, with less time spent at surface in the higher CO_2 treatments (Table 2). Similarly, tests for proportion time spent in the middle and bottom depth bins also showed differences between treatment groups (KW, $p_{mid} = 0.001$, $p_{bottom} = 0.002$), wherein the 1300 ppm treatment group was distinct from the 1900 and 2200 ppm treatment groups, with more time spent in the middle and bottom depth bins in the higher CO_2 treatments

(Table 2). This reflects the extremely low variance in the 1300 ppm treatment group compared to all other treatments in all depth bins ($\sigma^2 \leq 0.001$, Table 3). Variance did not significantly increase with CO_2 level in the top or bottom depth bin, but showed an increasing trend with increasing CO_2 level in the middle depth bin ($R^2 = 0.609$, Table 3). Despite notable individual variability across treatments and interannual variability in response, the experiment indicated that squid paralarvae spent less time at the surface in CO_2 treatments of 1900 and 2200 ppm overall (Fig. 2C).

Experiment 2: 3D Metrics

In the 3D system, paralarvae showed no difference in the proportion of time spent in any depth bin across CO_2 treatments (KW, $p_{top} = 0.1094$, $p_{mid} = 0.0568$, $p_{bottom} = 0.0694$, Table 4) in all trials of both 2014 and 2015, nor were there any notable trends in the variance for this metric (Table 5). The proportion of time spent in the top depth bin showed a weak, non-significant decrease with increasing pCO_2 ($R^2 = 0.6455$) and proportions of time spent in the mid and bottom depth bins showed corresponding, non-significant increasing trends with increasing acidification (Table 4).

Of the 3D metrics measured for the paralarvae, total distance (KW, $p = 0.0342$), average velocity (KW, $p = 0.0354$), average positive vertical velocity (KW, $p = 0.0126$), and average negative vertical velocity (KW, $p = 0.0028$) showed significant effects of CO_2 treatment (Table 4). Dunn's posthoc test revealed the difference to be between the 400 and 1000 ppm groups for all of these metrics (Table 6). Average velocity was slightly higher in the 400 ppm treatment level, 9.4 mm s^{-1} (8.2 - 11.7), compared to the other CO_2 treatments: 8.0 mm s^{-1} (7.1 - 9.3), 8.3 mm s^{-1} (7.6 - 9.9), and 8.2 mm s^{-1} (7.0 - 9.7) for 1000, 1600, and 2200 ppm, respectively (Table

4). A linear fit (R^2 = 0.4591) of the median average velocities across treatments demonstrates this potential decreasing trend with increasing pCO_2. The step-wise nature of this trend is reflected in the average positive and negative vertical velocity values (Table 4), while the horizontal component of the velocity showed a significant fit to a linear decreasing trend (R^2 = 0.9798, p = 0.0101) rather than any significant differences between treatments (KW, p = 0.1945). Percent time active, as assessed in the ethological work, also followed a significant decreasing linear trend (R^2 = 0.9798, p = 0.0077), without significant differences between groups (KW, p = 0.242).

Analyzed individuals exhibited the expected, stereotypical motion of hatchling paralarvae, swimming with repeated, and dominantly vertical, jetting motions (Fig. 3). Average jet velocity was highest in the 400 ppm treatment, 17.6 mm s^{-1} (14.2 - 19.6), and notably, but not significantly (KW, p = 0.1192) lower, in the 1000, 14.9 mm s^{-1} (13.1 - 16.5), 1600, 14.7 mm s^{-1} (13.0 - 16.9), and 2200 ppm, 15.1 mm s^{-1} (12.5 - 17.9) treatments. Peak velocity was highest in the 400 ppm treatment, 139.6 mm s^{-1} (99.9 - 206.9), and the 1000 ppm treatment, 138.2 mm s^{-1} (78.8 - 228.7), notably lower in the 1600 ppm, 108.1 mm s^{-1} (86.4- 163.3), and 2200 ppm treatments, 123.9 mm s^{-1} (82.1 - 187.5), showing a weak decreasing linear trend (R^2 = 0.4578), but no statistical significance (KW, p = 0.4378). Vertical and horizontal peak velocities also show this pattern of more step-wise and weakly linear, non-significant decrease from 400 ppm (Table 4). Jetting rate, on the other hand, showed similar values between 400 ppm, 2.73 Jets s^{-1} (2.51 - 3.02), 1000 ppm, 2.70 Jets s^{-1} (2.51 - 2.89), and 1600 ppm, 2.72 Jets s^{-1} (2.47 - 2.85), and only decreased slightly at 2200 ppm, 2.63 Jets s^{-1} (2.38 - 2.81) (KW, p = 0.3436).

Three-dimensional polygons of volume transited, tortuosity paths, and turning angle distributions were also determined (Fig. 4). Volume traveled by the paralarvae during the

swimming recording was notably, but not significantly (KW, $p = 0.7416$) lower in the 2200 ppm treatment, 46,406 mm^3 (22,078 - 118,883), compared to the other treatments, 53,786 mm^3 (20,550 - 95,664), 65,076 mm^3 (33,647 - 125,970), and 53,315 mm^3 (30,734 - 103,950) for 400, 1000, and 1600 ppm respectively, and demonstrated a weakly decreasing linear trend ($R^2 = 0.4334$). Variance was high for volume transited across treatments (σ^2 range = 2.86×10^9 - 7.71×10^9, overall CV = 0.918) and appeared to increase with increasing CO_2 ($R^2 = 0.8710$, Table 5).

Average turning angle was highest in the 400 ppm treatment group, 56.53º (48.84º - 64.54º), whereas values were similar amongst the other treatments: 53.49º (48.45º - 62.04º), 52.05º (45.92º - 60.00º), and 52.30º (43.64º - 63.71º) for 1000, 1600, and 2200 ppm, respectively, resulting from a slightly higher occurrence of reversals in the 400 ppm group. Similar to other metrics, average turning angle was not statistically significant (KW, $p = 0.4334$), but still showed a slightly decreasing linear trend ($R^2 = 0.7863$). No apparent impacts of acidification on paralarval control of orientation were observed. Distributions of the turning angles from the entire paralarval path did not vary between treatments, except in the 120º - 130º bin where turns were rare (Average frequency of turns, 120 - 130º, all treatments < 0.025; $KW_{120\text{-}130}$, $p = 0.013$; KW, $p > 0.05$ for all other turning angle bins). All experimental paralarvae demonstrated primarily forward and reverse motions, due to the dominance of jetting, and a slightly higher frequency of shallow (10 - 40º) forward turns along their swimming paths.

Average tortuosity did not vary notably between CO_2 treatments (KW, $p = 0.6730$). It was highest in the 2200 ppm treatment, 3.63 (3.07 - 5.19), and lowest in the 1600 ppm treatment, 3.39 (2.92 - 4.51), showing a weakly increasing trend with increasing CO_2 ($R^2 = 0.4065$, Table 4).

Variance was higher in the 400 and 2200 ppm treatments than in the other CO_2 treatments for several metrics (total distance, average velocity, turning angle) (Table 5). Overall variability, as demonstrated by the CV for each metric, was highest in peak velocities, average vertical velocity components, volume transited, and average tortuosity (Table 5). Except for volume transited, as previously noted, and average jet velocity, which had an increasing trend in both variance and CV with increasing CO_2 (σ^2 R^2 = 0.6506, CV R^2 = 0.8647) variability did not fit an increasing or decreasing trend across CO_2 treatments for the 3D metrics (Table 5). Patterns of variance seen in the 3D metrics do not appear to align with variation in the total number of individuals recorded for each CO2 treatment (Table 1). Although individual paralarvae were quite variable over the course of their swimming path, medians and overall trends of the total dataset were consistent across the entire recorded swimming period (KW, $p > 0.05$ across 10-second time bins within CO_2 treatments for all 3D metrics) (Fig. 5).

Discussion

Paralarvae recorded in the 2D behavior arena demonstrated a decrease in time spent in the top, near-surface depth bin at the highest CO_2 concentrations tested. Squid paralarvae are negatively buoyant and "hop" with pulsed jetting to maintain their position in between sinks, the rate of which could decrease with decreased available energy (Seibel et al., 2000). Squid jetting comes at a high energetic cost, which has been proposed as a driver of their "live fast, die young" lifestyle and highlighted as a limitation in their ability to compete directly with fish (O'Dor & Webber, 1986). Propulsive efficiency, of just the jetting contraction phase, has been shown to be quite high in *D. pealeii* paralarvae, greater than 80%, decreasing with growth to the juvenile & adult phases (Bartol et al., 2008, 2009a). Modeled hydrodynamic efficiency for squid,

considering the whole jetting cycle, however, demonstrated that efficiency increases with growth from hatching to a peak efficiency of about 40% at 10 mm DML, decreasing slightly thereafter (Staaf et al., 2014). The decrease in time spent near the surface seen in high CO_2-exposed paralarvae in the 2D analysis may have been caused by a reallocation of available energy by these paralarvae towards stress response resulting in decreased swimming activity, a reduction in jetting efficiency due to slightly smaller mantle size (seen in Kaplan et al., 2013), or a combination thereof, resulting in increased time spent sinking. Limitations in the analytical power of the 2D system prevented further disentanglement of these factors.

The significant reductions in average 3D velocity and average positive vertical velocity, as well as the significant decreasing trend in paralarval activity from the 3D system, support the idea that acidification impacts the energetics of the paralarvae, even if effects are slight. Other observed metrics of 3D swimming activity did not demonstrate significant shifts across CO_2 levels, but exhibited decreasing patterns with increasing CO_2 exposure, further suggesting a subtle impact of acidification on the energetics and dynamics of swimming. Hypercapnia has been shown to depress energy expenditure rates in embryonic and pre-hatchling cuttlefish, *Sepia officinalis* (Rosa et al., 2013). Adults and juveniles of this species appear capable of withstanding chronic acidification through a system of branchial acid-base transporters, but embryos were seen to a downregulate ion regulatory and metabolic genes under increased acidification (Hu et al., 2011). Ion pump activities were seen to be even lower in the embryos and paralarvae of a Loliginid squid, *Loligo vulgaris*, than in *S. officinalis*, suggesting a greater pH sensitivity in this taxa (Hu et al., 2010). However, embryos of another squid, *Sepioteuthis lessoniana*, upregulated genes of a proton secretion pathway under severe chronic acidification (pH_{nbs} = 7.31) demonstrating the potential for a powerful homeostatic response (Hu et al., 2013). Given that

cephalopod eggs naturally become acidified due to embryonic respiration over the course of development, it is possible that, while variable, a general pH resilience is a conserved feature of the class, which may serve to explain the weakness in OA responses seen here (Gutowska & Melzner, 2009; Long et al., 2016).

The OA effects on vertical swimming in 2013 and decreasing trends in 3D swimming behaviors in 2014 demonstrated a remarkable resilience, requiring intense, chronic exposures (> 1900 ppm) to acidification that *D. pealeii* should at most experience acutely in estuarine environments (Jacobson, 2005; Baumann et al., 2014). These levels of acidification are predicted in models only under a high emissions scenario after several hundred years (Caldeira & Wickett, 2003). Early physiological work exposing adult *D. pealeii* to hypercapnia noted the remarkable CO_2 tolerance of this species, suggesting that even with the Bohr effect, decreased pH reducing oxygen carrying capacity of their hemocyanin, they would not be significantly stressed unless exposed to concurrent hypoxia (Redfield & Goodkind, 1929). Embryos of the California market squid, *Doryteuthis opalescens*, which naturally experience sporadic pH reduction (down to 7.65) due to upwelling, showed development delay and smaller statoliths under a combined regime of OA (pH 7.57) and hypoxia (80µM), while under only decreased pH (7.56) showed a reduced yolk volume, but larger statoliths compared to hypoxia alone (Navarro et al., 2016). Given the substantial acid-base balancing machinery of cephalopods, it is possible that if subtle effects of acidification are seen, particularly in relation to energy and activity, it is due to a slightly reduced oxygen availability owing to the pH sensitivity of their hemocyanin, but that they are otherwise fairly resistant to acidification in a well oxygenated system (Hu et al., 2010; Seibel, 2013).

While the 2013 2D depth results showed a clear impact of high, chronic acidification on paralarval swimming behavior (Fig. 2A), no significant effect of pCO_2 on paralarval swimming

depth was seen in the 2014 2D trial and all subsequent 3D trials (run in 2014 & 2015) (Fig. 2B, Table 4), indicating a possible interannual or cohort-based variance in the strength of embryonic and paralarval response to this stressor. Seasonal cohorts of *L. vulgaris* eggs were shown to respond differentially to warming and OA, with the summer clutches showing greater sensitivity (Rosa et al., 2014). Murray et al. have demonstrated intraspecies seasonal variability in OA stress response for the Atlantic silverside, *Menidia menidia*, dependent on parental exposure and offspring conditioning (2014). The annual *D. pealeii* breeding cycle in Vineyard Sound is known to have some weak seasonal structuring with the earliest mating (April-May) involving robust two-year olds, while the rest of the breeding season is dominated by the previous year-class, however our data does not correlate with any clear seasonal signal (Arnold et al., 1974). Squid populations have been noted to demonstrate interannual variability, potentially as a plastic response of the year-class to environmental influence (Pecl et al., 2004). It is possible that an organism as plastic and fast-lived as *D. pealeii* could exhibit differential responses to stressors dependent on the experiences of the year-class and on how those adults condition their resultant offspring (Summers, 1971).

Considerable variability in behavior and response was seen individually within the paralarvae, both overall (Fig. 5) and across CO_2 treatments (Table 3, Table 5). Seemingly high variance may be partly due to moderate sample sizes in some treatments (Table 1). However, the distributions of variance across CO_2 treatments, and the high coefficients of variation for many 3D metrics, indicate a more prominent effect of individual variability (Table 5). Complexity and plasticity are hallmarks of the cephalopods, and individual variability is a strong benefit for fast-lived, highly fecund, r-selected organisms such as squid, as it provides adaptive flexibility in the face of rapid environmental change (Herke & Foltz, 2002; Pecl et al., 2004). While variability

between cohorts of eggs is likely due to differences in parentage, variability within a clutch is an effect either of differential fathership and/or maternal condition (Buresch et al., 2001, 2009; Steer et al., 2004). Intracapsular variability within a maternal clutch has been noted in the elemental composition of statoliths, DML, and yolk volume in late stage *D. opalescens* embryos (Navarro et al., 2014, 2016). Given the complexity of squid parentage, differential parental conditioning and any resultant epigenetic effects might also express as differential responses or behaviors, particularly when dealing with a stressor, as is seen in other marine species (Buresch et al., 2001; Miller et al., 2012; Putnam & Gates, 2015). Maternal variation in transmitted yolk content could have impacts on both the paralarval energy budget and their specific gravity, both of which could translate to swimming behaviors (Vidal et al., 2002a; Martins et al., 2010). Embryo position in the egg capsule itself, and the resultant exposure to differential levels of hypoxia and acidification over development, could also explain the dynamic variability in individual swimming behaviors and activities seen in our experiment (Long et al., 2016).

It is likely that our power to see effects caused by OA was reduced by this intense individual variability and the logistical challenge of acquiring a large enough sample size of useable paralarvae videos. Differences in the 2D system were only seen between those treatment groups with either a substantial sample size of useable videos (400, 1900, and 2200 ppm, Table 1) or a particularly low variance (1300 ppm, Table 3). The videos resulting from the cubic arena provided substantially clearer imagery and allowed both for better observation and tracking of the squid paralarvae (Fig. 3, Fig. 4). An advantage of the new methodology implemented here is that it is easily set up and repeated. We were limited primarily by our organism's breeding window, the low ratio, for our paralarvae, of useable videos to videos taken, and the time needed for experimentation and processing (Table 1)(Vecchione, 1981; Hastie et al., 2009).

Three-dimensional positional data acquired through observer corrected automated tracking in Tracker and processing in the 3D model equations described above resulted in clear tracks for each individual, similar to those determined by other established methods (Cachat et al., 2011b). Individual tracked paths produced by the system provide a powerful basis for analyzing movement patterns in marine and aquatic organisms. Total distance traveled and average velocity of the paralarvae were significantly different between the 400 and 1000 ppm groups, but most of the 3D metrics examined demonstrated only weakly decreasing trends with increasing CO_2 (Table 4). Average velocities for *D. pealeii* paralarvae recorded from the 3D system, 8.3 mm s^{-1} ± 2.5 (median ± SD), fall within, but on the low end, of the range previously reported for the species during mantle contraction, 6.6 – 30.5 mm s^{-1} (Bartol et al., 2009a). Limitations in these metrics may arise from the general, undirected swimming of the organisms. All the animals studied swam at about the same rate and for the same general distance; however, the absence of flow, predators, prey, conspecifics, or other major sensory cues throughout these tests should be noted. It is possible that potential acidification effects in the 3D swimming system did not emerge, both because of the high multi-scale variability and because the paralarvae were not sufficiently challenged in their motion. Sensory-driven experiments taking advantage of the squid paralarvae's innate photopositivity as a target may better elucidate stress effects by coercing the organism into predictable, directed motion.

Both arenas used likely enacted some influence over the behavior of the paralarvae. Both systems only allowed for a still water experimentation regime and did not provide analysis of the natural impacts of turbulence and flow that other methods, particularly DPIV, are capable of (Fuchs et al., 2004; Wheeler et al., 2015). Stillwater also resulted in a flat surface layer, which was necessary for filming from above, but also allowed for the influence of surface tension,

which was found to entrain paralarvae in the meniscus of the 2D system, and has been shown in other studies to influence the speed and survival of marine larvae (Hidu & Haskin, 1978; Yamaoka et al., 2000). Paralarval *D. pealeii* do not live in a still water environment, but instead navigate the dynamic surface ocean; although their precise behaviors are not well known (Vecchione et al., 2001; Barón, 2003; Jacobson, 2005). Therefore, while the system was effective at exploring fundamental, physiologically-driven differences in hatchling swimming capability it does not directly reflect how paralarval swimming behaviors might shift in response to OA in the natural system or throughout ontogeny.

This study set out to examine the potential impacts of developmental exposure to OA on the swimming behavior of hatchling squid paralarvae. The study required and inspired the development of a novel, simple, and feasible system for recording, tracking, and analyzing the 3D motion of a motile marine larvae. Early results demonstrated an impact of high CO_2 exposures on paralarval activity and vertical positioning. Measured in the 3D system, average velocity and average positive vertical velocity showed significant decreases from ambient, 400 ppm, to 1000 ppm, while horizontal velocity showed a significantly decreasing trend further indicating an impact of OA on hatchling energetics. However, most metrics only demonstrated subtle, nonsignificant, decreasing trends with decreased pH, supporting the idea that acidification may be a weak stressor in cephalopods. Notable individual variability, as well as potential interannual and/or cohort scale variability, was also seen in the response to acidification, indicating a substantial plasticity and general pH resilience for the population. Further study into the physiological tolerances and behavioral responses of this taxon would require incorporating higher CO_2 levels, beyond 2200 ppm, or the introduction of compounding stressors in a multifactor design. Replication of this and related stress experiments across multiple years would

also be required in order to better describe the patterns and drivers of individual, intra-annual, and interannual variabilities. The 3D model system has potential utility in a wide variety of applications, including complex tracking of aquatic or marine larvae from other taxa, tracking of multiple individuals within the same arena, predator-prey interactions, as well as sensory studies. The range of organismal responses to anthropogenically induced global ocean change continues to grow in diversity and complexity as more taxa and stressors are examined. Improvements in the accessibility of methods to address this ever-expanding field of questions are necessary in order to facilitate and support this substantial effort.

References

Arkhipkin, A. I., & V. A. Bizikov, 2000. Role of the statolith in functioning of the acceleration receptor system in squids and sepioids. Journal of Zoology 250: 31–55.

Arnold, J. M., W. C. Summers, D. L. Gilbert, R. S. Manalis, N. W. Daw, & R. J. Lasek, 1974. A guide to laboratory use of the squid Loligo pealei. .

Barón, P. J., 2003. The paralarvae of two South American sympatric squid: Loligo gahi and Loligo sanpaulensis. Journal of Plankton Research 25: 1347–1358.

Bartol, I. K., P. S. Krueger, W. J. Stewart, & J. T. Thompson, 2009a. Pulsed jet dynamics of squid hatchlings at intermediate Reynolds numbers. The Journal of Experimental Biology 212: 1506–1518.

Bartol, I. K., P. S. Krueger, W. J. Stewart, & J. T. Thompson, 2009b. Hydrodynamics of pulsed jetting in juvenile and adult brief squid Lolliguncula brevis: evidence of multiple jet “modes” and their implications for propulsive efficiency. The Journal of Experimental Biology 212: 1889–1903.

Bartol, I. K., P. S. Krueger, J. T. Thompson, & W. J. Stewart, 2008. Swimming dynamics and propulsive efficiency of squids throughout ontogeny. Integrative and Comparative Biology 48: 720–733.

Baumann, H., R. B. Wallace, T. Tagliaferri, & C. J. Gobler, 2014. Large Natural pH, CO2 and O2 Fluctuations in a Temperate Tidal Salt Marsh on Diel, Seasonal, and Interannual Time Scales. Estuaries and Coasts .

Beck, M. W., K. L. Heck, K. W. Able, D. L. Childers, D. B. Eggleston, B. M. Gillanders, B. Halpern, C. G. Hays, K. Hoshino, T. J. Minello, R. J. Orth, P. F. Sheridan, & M. P. Weinstein, 2001. The Identification, Conservation, and Management of Estuarine and Marine Nurseries for Fish and Invertebrates. BioScience 51: 633.

Benoit-Bird, K. J., & W. F. Gilly, 2012. Coordinated nocturnal behavior of foraging jumbo squid Dosidicus gigas. Marine Ecology Progress Series 455: 211–228.

Boisclair, D., 1992. An Evaluation of the Stereocinematographic Method to Estimate Fish Swimming Speed. Canadian Journal of Fisheries and Aquatic Sciences 49: 523–531.

Budick, S. A., & D. M. O'Malley, 2000. Locomotor repertoire of the larval zebrafish: swimming, turning and prey capture. The Journal of Experimental Biology 203: 2565–2579.

Buresch, K. C., M. R. Maxwell, M. R. Cox, & R. T. Hanlon, 2009. Temporal dynamics of mating and paternity in the squid Loligo pealeii. Marine Ecology Progress Series 387: 197–203.

Buresch, K. M., R. T. Hanlon, M. R. Maxwell, & S. Ring, 2001. Microsatellite DNA markers indicate a high frequency of multiple paternity within individual field-collected egg capsules of the squid Loligo pealeii. Marine Ecology Progress Series 210: 161–165.

Byrne, M., 2011. Impact of ocean warming and ocean acidification on marine invertebrate life history stages : Vulnerabilities and potential for persistence in a changing ocean. Oceanogr. Mar. Biol. Annu. Rev. 49: 1–42.

Cachat, J. M., P. R. Canavello, S. I. Elkhayat, B. K. Bartels, P. C. Hart, M. F. Elegante, C. Esther, A. L. Laffoon, W. A. M. Haymore, D. H. Tien, A. K. Tien, S. Mohnot, & A. V Kalueff, 2011a. Chapter 16: Deconstructing Adult Zebrafish Behavior with Swim Trace Visualizations In Kalueff, A. V., & J. M. Cachat (eds), Zebrafish Neurobehavioral Protocols. : 191–201.

Cachat, J., A. Stewart, E. Utterback, P. Hart, S. Gaikwad, K. Wong, E. Kyzar, N. Wu, & A. V. Kalueff, 2011b. Three-dimensional neurophenotyping of adult zebrafish behavior. PLoS ONE 6.

Caldeira, K., & M. E. Wickett, 2003. Oceanography: anthropogenic carbon and ocean pH. Nature 425: 365.

Coughlin, D. J., J. R. Strickler, & B. Sanderson, 1992. Swimming and Search Behavior in Clownfish, Amphiprion-Perideraion, Larvae. Animal Behaviour 44: 427–440.

Doney, S. C., V. J. Fabry, R. A. Feely, & J. A. Kleypas, 2009. Ocean acidification: the other CO2 problem. Annual Review of Marine Science 1: 169–192.

Fuchs, H. L., L. S. Mullineaux, & A. R. Solow, 2004. Sinking behavior of gastropod larvae (Ilyanassa obsoleta) in turbulence. Limnology and Oceanography 49: 1937–1948.

Gledhill, D. ., M. . White, J. Salisbury, H. Thomas, I. Misna, M. Liebman, B. Mook, J. Grear, A. C. Candelmo, R. C. Chambers, C. J. Gobler, C. W. Hunt, A. L. King, N. N. Price, S. R. Signorini, E. Stancioff, C. Stymiest, R. A. Wahle, J. D. Waller, N. D. Rebuck, & Z. A. Wang, 2015. Ocean and coastal acidification off New England and Nova Scotia. Oceanography 28: 182–197.

Guppy, M., & P. Withers, 1999. Metabolic depression in animals: physiological perspectives and biochemical generalizations. Biological reviews of the Cambridge Philosophical Society 74: 1–40.

Gutowska, M. A., & F. Melzner, 2009. Abiotic conditions in cephalopod (Sepia officinalis) eggs: Embryonic development at low pH and high pCO2. Marine Biology 156: 515–519.

Gutowska, M. A., F. Melzner, M. Langenbuch, C. Bock, G. Claireaux, & H. O. Pörtner, 2010. Acid–base regulatory ability of the cephalopod (Sepia officinalis) in response to environmental hypercapnia. Journal of Comparative Physiology B 180: 323–335.

Hanlon, R., J. Bidwell, & R. Tait, 1989. Strontium is required for statolith development and thus normal swimming behaviour of hatchling cephalopods. Journal of Experimental Biology 141:

187–195.

Hanlon, R. T., R. F. Hixon, & W. H. Hulet, 1983. Survival, growth, and behavior of the loliginid squids Lologi plei, Loligo pealei, and Lolliguncula brevis (Mollusca: Cephalopoda) in closed sea water systems. Biology Bulletin 637–685.

Hastie, L. C., G. J. Pierce, J. Wang, I. Bruno, & A. Moreno, 2009. Cephalopods in the North-Eastern Atlantic: Species, Biogeography, Ecology, Exploitation and Conservation. Oceanography and Marine Biology: An Annual Review 47: 111–190.

Haury, L., & D. Weihs, 1976. Energetically efficient swimming behavior of negatively buoyant zooplankton. Limnology and Oceanography 21: 797–803.

Herke, S. W., & D. W. Foltz, 2002. Phylogeography of two squid (Loligo pealei and L. plei) in the Gulf of Mexico and northwestern Atlantic Ocean. Marine Biology 140: 103–115.

Hidu, H., & H. H. Haskin, 1978. Swimming speeds of oyster larvae Crassostrea virginica in different salinities and temperatures. Estuaries 1: 252–255.

Honisch, B., A. Ridgwell, D. N. Schmidt, E. Thomas, S. J. Gibbs, A. Sluijs, R. Zeebe, L. Kump, R. C. Martindale, S. E. Greene, W. Kiessling, J. Ries, J. C. Zachos, D. L. Royer, S. Barker, T. M. Marchitto, R. Moyer, C. Pelejero, P. Ziveri, G. L. Foster, & B. Williams, 2012. The Geological Record of Ocean Acidification. Science 335: 1058–1063.

Hu, M. Y., J.-R. Lee, L.-Y. Lin, T.-H. Shih, M. Stumpp, M.-F. Lee, P.-P. Hwang, & Y.-C. Tseng, 2013. Development in a naturally acidified environment: Na+/H+-exchanger 3-based proton secretion leads to CO2 tolerance in cephalopod embryos. Frontiers in zoology 10: 51.

Hu, M. Y., E. Sucre, M. Charmantier-Daures, G. Charmantier, M. Lucassen, N. Himmerkus, & F. Melzner, 2010. Localization of ion-regulatory epithelia in embryos and hatchlings of two cephalopods. Cell and Tissue Research 339: 571–583.

Hu, M. Y., Y.-C. Tseng, M. Stumpp, M. A. Gutowska, R. Kiko, M. Lucassen, & F. Melzner, 2011. Elevated seawater PCO_2 differentially affects branchial acid-base transporters over the course of development in the cephalopod Sepia officinalis. American journal of physiology. Regulatory, integrative and comparative physiology 300: R1100–R1114.

Hunsicker, M. E., & T. E. Essington, 2008. Evaluating the potential for trophodynamic control of fish by the longfin inshore squid (Loligo pealeii) in the Northwest Atlantic Ocean. Canadian Journal of Fisheries and Aquatic Sciences 65: 2524–2535.

Jacobson, L. D., 2005. Longfin Inshore Squid, *Loligo pealeii*, Life History and Habitat Characteristics. NOAA Technical Memorandum NMFS-NE.

Kaplan, M. B., T. A. Mooney, D. C. McCorkle, & A. L. Cohen, 2013. Adverse Effects of Ocean Acidification on Early Development of Squid (Doryteuthis pealeii). PLOS ONE 8.

Klimley, A. P., & S. T. Brown, 1983. Stereophotography for the field biologist: measurement of lengths and three-dimensional positions of free-swimming sharks. Marine Biology 74: 175–185.

Long, M. H., T. A. Mooney, & C. Zakroff, 2016. Extreme low oxygen and decreased pH conditions naturally occur within developing squid egg capsules. Marine Ecology Progress Series 550: 111–119.

Macy III, W. K., 1982. Feeding Patterns of the Long-Finned Squid, Loligo pealei, in New England Waters. Biological Bulletin 162: 28–38.

Macy III, W. K., & J. K. T. Brodziak, 2001. Seasonal maturity and size at age of Loligo pealeii in waters of southern New England. ICES Journal of Marine Science 58: 852–864.

Martins, R. S., M. J. Roberts, N. Chang, P. Verley, C. L. Moloney, & E. a G. Vidal, 2010. Effect of yolk utilization on the specific gravity of chokka squid (Loligo reynaudii) paralarvae: Implications for dispersal on the Agulhas Bank, South Africa. ICES Journal of Marine Science 67: 1323–1335.

Maxwell, M. R., & R. T. Hanlon, 2000. Female reproductive output in the squid Loligo pealeii: Multiple egg clutches and implications for a spawning strategy. Marine Ecology Progress Series 199: 159–170.

McCorkle, D. C., C. Weidman, & A. L. Cohen, 2012. Time series of pCO2, pH, and aragonite saturation state in Waquoit Bay National Estuarine Research Reserve: "estaurine acidification" and shellfish. Ocean Sciences Meeting. Salt Lake City, UT.

McMahon, J. J., & W. C. Summers, 1971. Temperature effects on the developmental rate of squid (Loligo pealei) embryos. The Biological Bulletin 141: 561–567.

Messenger, J. B., 1970. Optomotor responses and nystagmus in intact, blinded and statocystless cuttlefish (Sepia officinalis L.). The Journal of experimental biology 53: 789–796.

Miller, G. M., S.-A. Watson, J. M. Donelson, M. I. McCormick, & P. L. Munday, 2012. Parental environment mediates impacts of increased carbon dioxide on a coral reef fish. Nature Climate Change Nature Publishing Group 2: 858–861.

Murray, C. S., A. Malvezzi, C. J. Gobler, & H. Baumann, 2014. Offspring sensitivity to ocean acidification changes seasonally in a coastal marine fish. Marine Ecology Progress Series 504: 1–11.

Navarro, M. O., E. E. Bockmon, C. A. Frieder, J. P. Gonzalez, & L. A. Levin, 2014. Environmental pH, O2 and Capsular Effects on the Geochemical Composition of Statoliths of Embryonic Squid Doryteuthis opalescens. Water 2233–2254.

Navarro, M. O., G. T. Kwan, O. Batalov, C. Y. Choi, N. T. Pierce, & L. A. Levin, 2016. Development of Embryonic Market Squid, Doryteuthis opalescens, under Chronic Exposure to Low Environmental pH and [O2]. Plos One 11.

O'Dor, R. K., & D. M. Webber, 1986. The constraints on cephalopods: why squid aren't fish. Canadian Journal of Zoology 64: 1591–1605.

Pecl, G. T., N. A. Moltschaniwskyj, S. R. Tracey, & A. R. Jordan, 2004. Inter-annual plasticity of squid life history and population structure: Ecological and management implications. Oecologia 139: 515–524.

Putnam, H. M., & R. D. Gates, 2015. Preconditioning in the reef-building coral Pocillopora damicornis and the potential for trans-generational acclimatization in coral larvae under future climate change conditions. Journal of Experimental Biology 218: 2365–2372.

Redfield, A. C., & R. Goodkind, 1929. The Significance of the Bohr Effect in the Respiration and Asphyxiation of the squid, Loligo pealei. Journal of Experimental Biology 6: 340–349.

Robin, J. P., M. Roberts, L. Zeidberg, I. Bloor, A. Rodriguez, F. Briceño, N. Downey, M. Mascaró, M. Navarro, A. Guerra, J. Hofmeister, D. D. Barcellos, S. A. P. Lourenço, C. F. E. Roper, N. A. Moltschaniwskyj, C. P. Green, & J. Mather, 2014. Transitions during cephalopod

life history: The role of habitat, environment, functional morphology and behaviour. Advances in Marine Biology.

Rosa, R., K. Trübenbach, M. S. Pimentel, J. Boavida-Portugal, F. Faleiro, M. Baptista, G. Dionísio, R. Calado, H. O. Pörtner, & T. Repolho, 2014. Differential impacts of ocean acidification and warming on winter and summer progeny of a coastal squid (Loligo vulgaris). The Journal of Experimental Biology 217: 518–525.

Rosa, R., K. Trübenbach, T. Repolho, M. Pimentel, F. Faleiro, J. Boavida-Portugal, M. Baptista, V. M. Lopes, G. Dionísio, M. C. Leal, R. Calado, & H. O. Pörtner, 2013. Lower hypoxia thresholds of cuttlefish early life stages living in a warm acidified ocean. Proceedings of the Royal Society B: Biological Sciences 280: 20131695.

Seibel, B. A., 2013. The jumbo squid, Dosidicus gigas (Ommastrephidae), living in oxygen minimum zones II: Blood-oxygen binding. Deep-Sea Research Part II: Topical Studies in Oceanography Elsevier 95: 139–144.

Seibel, B. A., F. G. Hochberg, & D. B. Carlini, 2000. Life history of Gonatus onyx (Cephalopoda: Teuthoidea): deep-sea spawning and post-spawning egg care. Marine Biology 137: 519–526.

Shashar, N., & R. T. Hanlon, 2013. Spawning behavior dynamics at communal egg beds in the squid Doryteuthis (Loligo) pealeii. Journal of Experimental Marine Biology and Ecology 447: 65–74.

Sokolova, I. M., 2013. Energy-limited tolerance to stress as a conceptual framework to integrate the effects of multiple stressors. Integrative and Comparative Biology 53: 597–608.

Sokolova, I. M., M. Frederich, R. Bagwe, G. Lannig, & A. A. Sukhotin, 2012. Energy homeostasis as an integrative tool for assessing limits of environmental stress tolerance in aquatic invertebrates. Marine Environmental Research 79: 1–15.

Staaf, D. J., W. F. Gilly, & M. W. Denny, 2014. Aperture effects in squid jet propulsion. The Journal of Experimental Biology 217: 1588–1600.

Stamhuis, E., & J. Videler, 1995. Quantitative flow analysis around aquatic animals using laser sheet particle image velocimetry. The Journal of Experimental Biology 198: 283–294.

Steer, M. A., N. A. Moltschaniwskyj, D. S. Nichols, & M. Miller, 2004. The role of temperature and maternal ration in embryo survival: Using the dumpling squid Euprymna tasmanica as a model. Journal of Experimental Marine Biology and Ecology 307: 73–89.

Summers, W. C., 1971. Age and growth of Loligo pealei, a population study of the common Atlantic coast squid. Biological Bulletin 141: 189–201.

Summers, W. C., J. J. McMahon, & G. N. P. A. Ruppert, 1974. Studies on the Maintenance of Adult Squid (Loligo Peali). II. Empirical Extensions. Biological Bulletin 146: 291–301.

Vecchione, M., 1981. Aspects of the early life history of Loligo pealeii (Cephalopoda; Myopsida). Journal of Shellfish Research 1: 171–180.

Vecchione, M., C. F. E. Roper, M. J. Sweeney, & C. C. Lu, 2001. Distribution , Relative Abundance and Developmental Morphology of Paralarval Cephalopods in the Western North Atlantic Ocean Paralarval Cephalopods in the. NOAA Technical Reports NMFS 152:.

Vidal, E. A. G., F. P. DiMarco, J. H. Wormuth, & P. G. Lee, 2002a. Influence of Temperature

and Food Availability on Survival , Growth and Yolk Utilization in Hatchling Squid. Bulletin of Marine Science 71: 915–931.

Vidal, E. A. G., F. P. DiMarco, J. H. Wormuth, & P. G. Lee, 2002b. Optimizing rearing conditions of hatchling loliginid squid. Marine Biology 140: 117–127.

Villanueva, R., C. Nozais, & S. V. Boletzky, 1997. Swimming behaviour and food searching in planktonic Octopus vulgaris Cuvier from hatching to settlement. Journal of Experimental Marine Biology and Ecology 208: 169–184.

Vogel, S., 1981. Life in Moving Fluids: The Physical Biology of Flow. Princeton University Press, Princeton, New Jersey.

Wang, Z. A., R. Wanninkhof, W.-J. Cai, R. H. Byrne, X. Hu, T.-H. Peng, & W.-J. Huang, 2013. The marine inorganic carbon system along the Gulf of Mexico and Atlantic coasts of the United States : Insights from a transregional coastal carbon study. Limnology and Oceanography 58: 325–342.

Wassersug, R., & K. von Seckendorf Hoff, 1985. The kinematics of swimming in anuran larvae. Journal of experimental biology 119: 1–30.

Wheeler, J. D., K. R. Helfrich, E. J. Anderson, B. McGann, P. Staats, A. E. Wargula, K. Wilt, & L. S. Mullineaux, 2013. Upward swimming of competent oyster larvae Crassostrea virginica persists in highly turbulent flow as detected by PIV flow subtraction. Marine Ecology Progress Series 488: 171–185.

Wheeler, J. D., K. R. Helfrich, E. J. Anderson, & L. S. Mullineaux, 2015. Isolating the hydrodynamic triggers of the dive response in eastern oyster larvae. Limnology and Oceanography.

Yamaoka, K., T. Nanbu, M. Miyagawa, T. Isshiki, & a. Kusaka, 2000. Water surface tension-related deaths in prelarval red-spotted grouper. Aquaculture 189: 165–176.

York, C. A., & I. K. Bartol, 2016. Anti-predator behavior of squid throughout ontogeny. Journal of Experimental Marine Biology and Ecology Elsevier B.V. 480: 26–35.

Zeidberg, L. D., G. Isaac, C. L. Widmer, H. Neumeister, & W. F. Gilly, 2011. Egg capsule hatch rate and incubation duration of the California market squid, Doryteuthis (=Loligo) opalescens: Insights from laboratory manipulations. Marine Ecology 32: 468–479.

Table 1. Description of behavioral experiments divided by arena type, year, and trial. Seawater chemistry of CO_2 treatments for experimental squid egg capsule rearing cups (n = 4 cups per treatment level, 3 with squid egg capsules and 1 control) for all 2013, 2014, & 2015 behavior trials are provided. Values are reported as means with standard deviation. The total number of videos taken for each treatment is listed. Of the videos taken, only subsets of useable videos, those in which paralarvae were behaving normally and were either visually assessable or trackable by software, were used in the subsequent analyses

Arena	Year	Trial	Laying Date	Treatment CO_2 (ppm)	Temp (°C)	pH_{total}	Salinity	A_T (mmol $kgSW^{-1}$)	Ω_{Arag}	pCO_2 (ppm)	Videos Taken	Useable/Analyzed Videos		
												Depth Bins	Ethology	3D Tracks
2D	2013	1	03-Jul	Ambient (550)	20.83 (0.19)	7.88 (0.02)	31.40 (0.06)	2060.3 (12.5)	1.87 (0.08)	565.68 (43.90)	20	7	-	-
				1300	20.83 (0.19)	7.54 (0.01)	31.41 (0.03)	2064.7 (6.6)	0.93 (0.04)	1350.51 (43.55)	18	13	-	-
				2200	20.83 (0.19)	7.34 (0.01)	31.39 (0.05)	2064.9 (16.1)	0.60 (0.04)	2199.56 (173.47)	20	11	-	-
		2	11-Jul	850	20.46 (0.03)	7.66 (0.01)	31.26 (0.13)	2042.1 (30.3)	1.17 (0.03)	987.43 (20.30)	45	36	-	-
				1300	20.46 (0.03)	7.54 (0.03)	31.29 (0.07)	2051.6 (10.2)	0.90 (0.03)	1351.67 (34.26)	46	21	-	-
				2200	20.46 (0.03)	7.31 (0.01)	31.25 (0.13)	2047.1 (21.2)	0.54 (0.02)	2380.50 (70.62)	45	30	-	-
		4	07-Aug	400	19.97 (0.49)	7.93 (0.01)	31.51 (0.01)	2032.0 (20.0)	1.95 (0.00)	488.58 (10.50)	69	44	-	-
				1900	19.97 (0.49)	7.37 (0.00)	31.46 (0.02)	2015.8 (5.7)	0.59 (0.00)	2003.79 (12.84)	75	67	-	-
				2200	19.97 (0.49)	7.35 (0.01)	31.45 (0.02)	2028.1 (0.0)	0.56 (0.01)	2130.17 (40.31)	97	84	-	-
	2014	1	29-May	400	20.32 (0.18)	7.97 (0.02)	32.21 (0.13)	2188.2 (32.4)	2.27 (0.11)	471.27 (28.31)	46	27	-	-
				1500	20.32 (0.18)	7.55 (0.01)	32.17 (0.05)	2176.4 (33.4)	0.98 (0.04)	1403.10 (22.78)	47	15	-	-
				1700	20.32 (0.18)	7.48 (0.00)	32.17 (0.04)	2179.5 (20.7)	0.85 (0.02)	1635.81 (23.56)	43	21	-	-
				2200	20.32 (0.18)	7.40 (0.02)	32.12 (0.05)	2176.6 (22.3)	0.69 (0.03)	2001.40 (103.08)	62	18	-	-
3D	2014	2	02-Jul	400	20.65 (0.20)	7.99 (0.05)	32.37 (0.33)	2140.6 (18.3)	2.39 (0.21)	439.52 (58.83)	74	17	10	0
				1000	20.65 (0.20)	7.68 (0.01)	32.13 (0.23)	2137.9 (17.9)	1.28 (0.04)	982.22 (27.04)	45	13	11	4
				1600	20.65 (0.20)	7.49 (0.01)	32.18 (0.19)	2136.0 (18.2)	0.86 (0.03)	1565.44 (40.27)	79	25	12	3
				2200	20.65 (0.20)	7.44 (0.07)	32.13 (0.24)	2134.5 (20.2)	0.77 (0.12)	1787.99 (282.04)	40	9	11	4
		3	18-Jul	400	20.24(0.08)	7.99 (0.02)	31.84 (0.50)	2097.8 (19.5)	2.25 (0.08)	439.87 (24.74)	71	26	10	10
				1000	20.24(0.08)	7.70 (0.01)	31.88 (0.34)	2104.3 (19.6)	1.27 (0.04)	934.49 (34.46)	80	19	12	11
				1600	20.24(0.08)	7.49 (0.01)	31.99 (0.34)	2112.3 (37.8)	0.82 (0.02)	1562.37 (45.50)	77	17	10	10
				2200	20.24(0.08)	7.38 (0.03)	31.93 (0.37)	2104.9 (23.1)	0.65 (0.03)	2033.82 (136.79)	74	25	10	13
		4	05-Sep	400	20.73 (0.23)	8.00 (0.03)	32.75 (0.09)	2096.0 (19.4)	2.39 (0.12)	418.25 (31.45)	78	18	10	10
				1000	20.73 (0.23)	7.72 (0.03)	32.43 (0.16)	2090.1 (17.3)	1.38 (0.09)	856.00 (53.73)	91	18	11	11
				1600	20.73 (0.23)	7.56 (0.04)	32.42 (0.27)	2087.3 (13.9)	0.98 (0.08)	1290.21 (128.77)	78	17	10	11
				2200	20.73 (0.23)	7.40 (0.03)	32.43 (0.15)	2090.1 (19.8)	0.69 (0.05)	1909.49 (148.80)	69	17	10	12
	2015	1	22-May	400	20.36 (0.44)	7.98 (0.04)	33.10 (0.16)	2201.4 (18.7)	2.44 (0.18)	454.10 (51.43)	68	17	10	17
				1000	20.36 (0.44)	7.75 (0.02)	33.00 (0.10)	2189.7 (17.7)	1.53 (0.05)	828.19 (34.32)	42	16	10	12
				1600	20.36 (0.44)	7.58 (0.03)	32.97 (0.07)	2197.5 (19.8)	1.05 (0.06)	1313.09 (100.28)	30	15	10	16
				2200	20.36 (0.44)	7.46 (0.03)	32.99 (0.09)	2202.6 (20.7)	0.81 (0.05)	1770.29 (97.62)	55	13	10	13

Experiment	1	2

Table 2 Significant Dunn's posthoc test statistics for differences between CO_2 treatments within all depth bins examined. Data compiled from all trials of Experiment 1, $Q_{crit} = 3.12$

CO_2 Treatment (ppm)	1900 Top	2200 Top	1900 Mid	2200 Mid	1900 Bottom	1900 Bottom
400 Top	3.52	3.72	-	-	-	-
1300 Top	3.97	4.06	-	-	-	-
1300 Middle	-	-	3.21	3.36	-	-
1300 Bottom	-	-	-	-	3.58	3.74

Table 3 Variance of 2D depth bins per CO_2 level compiled over all trials of Experiment 1. R^2 are of fits of linear trend lines ($p > 0.05$ for all regressions)

σ^2	400 ppm	550 ppm	850 ppm	1300 ppm	1500 ppm	1700 ppm	1900 ppm	2200 ppm	R^2
2D Top	0.105	0.143	0.036	0.001	0.178	0.047	0.156	0.156	0.054
2D Middle	0.006	0.000	0.007	0.001	0.027	0.033	0.015	0.036	0.609
2D Bottom	0.091	0.129	0.023	0.000	0.117	0.005	0.156	0.116	0.015

Table 4 Values of the 3D swimming behavior metrics at each CO_2 treatment. Reported values are medians and IQR. Significant Kruskal-Wallis p values marked with * ($p < 0.05$). R^2 are of fits of linear trend lines. Significant regressions are marked with * ($p < 0.05$).

3D Metric	400 ppm	1000 ppm	1600 ppm	2200 ppm	KW p value	R^2
3D Top (% Frames)	0.95 (0.64 - 1.00)	0.88 (0.53 - 1.00)	0.92 (0.72 - 1.00)	0.81 (0.43 - 0.98)	0.1094	0.6455
3D Mid (% Frames)	0.01 (0.00 - 0.12)	0.07 (0.00 - 0.21)	0.05 (0.00 - 0.13)	0.06 (0.00 - 0.17)	0.0568	0.5030
3D Bottom (% Frames)	0.00 (0.00 - 0.16)	0.03 (0.00 - 0.17)	0.00 (0.00 - 0.08)	0.04 (0.00 - 0.30)	0.0694	0.3775
Ethology (% Active)	95.8 (88.1 - 100)	93.8 (86.5 - 100)	91.7 (68.5 - 99.4)	88.3 (69.2 - 100)	0.242	0.9847*
Total Distance (mm)	1128.7 (985.1 - 1403.9)	961.8 (855.7 - 1116.3)	997.9 (912.5 - 1187.9)	985.4 (840.2 - 1165.6)	0.0342*	0.4590
Average Velocity (mm s^{-1})	9.4 (8.2 - 11.7)	8.0 (7.1 - 9.3)	8.3 (7.6 - 9.9)	8.2 (7.0 - 9.7)	0.0354*	0.4590
Peak Velocity (mm s^{-1})	139.6 (99.9 - 206.9)	138.2 (78.8- 228.7)	108.1 (86.4 - 163.3)	123.9 (82.1 - 187.5)	0.4378	0.4578
Average Jet Velocity (mm s^{-1})	17.6 (14.2 - 19.6)	14.9 (13.1 - 16.5)	14.7 (13.0 - 16.9)	15.1 (12.5 - 17.9)	0.1192	0.5168
Jetting Rate (Jets s^{-1})	2.73 (2.51 - 3.02)	2.70 (2.51 - 2.89)	2.72 (2.47 - 2.85)	2.63 (2.38 - 2.81)	0.3436	0.6270
Average Vertical Velocity (mm s^{-1})	0.0 (-0.1 - 0.1)	0.0 (-0.1 - 0.3)	0.1 (0.0 - 0.4)	0.0 (-0.1 - 0.3)	0.1935	0.0678
Average Positive Vertical Velocity (mm s^{-1})	9.6 (7.9 - 10.6)	8.7 (6.8 - 9.3)	8.7 (7.1 - 9.6)	8.7 (7.4 - 9.7)	0.0126*	0.5540
Peak Vertical Velocity (mm s^{-1})	100.3 (75.0 - 150.6)	83.8 (60.6 - 138.3)	85.9 (62.4 - 127.0)	83.2 (66.6 - 106.9)	0.2584	0.6194

Average Negative Vertical Velocity (mm s^{-1})	-5.7 (-6.2 - -4.9)	-4.6 (-5.3 - -3.9)	-4.9 (-5.9 - -4.3)	-5.0 (-5.7 - -4.5)	0.0028*	0.2847
Minimum Vertical Velocity (mm s^{-1})	-83.5 (-122.2 - -62.8)	-63.1 (-118.6 - -44.5)	-74.9 (-101.4 - -54.6)	-79.9 (-117.1 - -49.5)	0.4982	0.0002
Average Horizontal Velocity (mm s^{-1})	4.6 (3.1 - 6.2)	4.3 (3.2 - 5.1)	3.7 (3.0 - 5.1)	3.4 (2.8 - 4.6)	0.1945	0.9798*
Peak Horizontal Velocity (mm s^{-1})	108.8 (72.7 - 138.8)	112.6 (61.2 - 174.5)	86.8 (58.6 - 107.5)	78.7 (67.8 - 149.1)	0.2712	0.8224
Volume Transited (mm^3)	53,786 (20,550 - 95,664)	65,076 (33,646 - 125,970)	53,314 (30,734 - 103,950)	46,406 (22,078 - 118,882)	0.7416	0.3207
Average Turn Angle (degrees)	56.53 (48.84 - 64.54)	53.49 (48.45 - 62.04)	52.05 (45.92 - 60.00)	52.30 (43.64 - 63.71)	0.4334	0.7863
Average Tortuosity	3.43 (3.00 - 4.79)	3.46 (2.97 - 4.35)	3.39 (2.92 - 4.51)	3.63 (3.07 - 5.19)	0.6730	0.4065

Table 5 Variance and coefficient of variation (CV) both per CO_2 treatment and overall for all of the 3D arena metrics. R^2 are of fits of linear trend lines ($p > 0.05$ for all regressions)

3D Metric		400 ppm	1000 ppm	1600 ppm	2200 ppm	R^2	Overall
3D Top (% Frames)	σ^2	0.1251	0.1007	0.0793	0.1162	0.0956	0.1073
	CV	0.473	0.440	0.352	0.503	0.0000	0.443
3D Mid (% Frames)	σ^2	0.0114	0.0210	0.0106	0.0131	0.0196	0.0143
	CV	1.48	1.16	1.22	1.09	0.7038	1.26
3D Bottom (% Frames)	σ^2	0.1107	0.0592	0.0585	0.1059	0.0048	0.0852
	CV	1.85	1.59	2.10	1.50	0.0637	1.77
Ethology (% Active)	σ^2	593	597	910	590	0.0607	685
	CV	0.284	0.291	0.393	0.303	0.1615	0.321
Total Distance (mm)	σ^2	99,095	58,994	65,760	106,467	0.0248	87,981
	CV	0.265	0.241	0.240	0.314	0.2961	0.275
Average Velocity (mm s^{-1})	σ^2	6.81	4.10	4.56	7.39	0.0305	6.08
	CV	0.264	0.241	0.240	0.314	0.3072	0.275
Peak Velocity (mm s^{-1})	σ^2	95,801	192,554	51,533	341,842	0.3596	177,644
	CV	1.20	1.56	1.33	1.89	0.3072	1.64
Average Jet Velocity (mm s^{-1})	σ^2	14.74	11.34	16.80	25.37	0.6506	17.99
	CV	0.221	0.221	0.258	0.314	0.8647	0.262
Jetting Rate (Jets s^{-1})	σ^2	0.1553	0.1556	0.0806	0.2751	0.2083	0.1745
	CV	0.145	0.150	0.106	0.208	0.1974	0.158
Average Vertical Velocity (mm s^{-1})	σ^2	0.067	0.158	0.102	0.126	0.1664	0.116
	CV	9.63	6.80	2.24	5.65	0.4854	4.61
Average Positive Vertical Velocity (mm s^{-1})	σ^2	4.87	5.19	3.15	4.75	0.1147	4.89
	CV	0.232	0.293	0.207	0.260	0.0001	0.258
Peak Vertical Velocity (mm s^{-1})	σ^2	13,692	45,967	4,545	4,056	0.2109	17,112
	CV	0.823	1.48	0.645	0.626	0.2097	1.07
Average Negative Vertical Velocity (mm s^{-1})	σ^2	2.02	1.65	1.50	2.22	0.0338	2.02
	CV	0.248	0.280	0.235	0.288	0.1519	0.274
Minimum Vertical Velocity (mm s^{-1})	σ^2	14,914	48,003	4,191	179,322	0.5174	65,185
	CV	0.988	1.73	0.718	2.68	0.3575	2.04
Average Horizontal Velocity (mm s^{-1})	σ^2	4.30	2.86	3.29	4.57	0.0389	3.86
	CV	0.429	0.378	0.414	0.523	0.4426	0.442
Peak Horizontal Velocity (mm s^{-1})	σ^2	94,830	158,355	49,637	185,639	0.1181	125,379
	CV	1.44	1.72	1.68	1.91	0.8284	1.76
Volume Transited (mm^3)	σ^2	2.86×10^9	4.39×10^9	4.56×10^9	7.71×10^9	0.8710	5.06×10^9

	CV	0.820	0.785	0.919	1.04	0.8015	0.918
Average Turn Angle (degrees)	σ^2	238.7	181.8	158.3	241.7	0.0020	211.0
	CV	0.262	0.248	0.236	0.281	0.0890	0.261
Average Tortuosity	σ^2	33.51	3.18	3.59	37.56	0.0076	20.20
	CV	1.18	0.430	0.478	1.09	0.0054	0.959

Table 6 Significant Dunn's posthoc test statistics for differences between CO_2 treatments in 3D metrics, $Q_{crit} = 2.631$

Metric: Treatment	400 ppm	1000 ppm	1600 ppm	2200 ppm
Total Distance (mm): 400 ppm	-	2.710	-	-
Average Velocity (mm s^{-1}): 400 ppm	-	2.700	-	-
Average Positive Vertical Velocity (mm s^{-1}): 400 ppm	-	3.200	-	-
Average Negative Vertical Velocity (mm s^{-1}): 400 ppm	-	3.741	-	-

Figure Captions

Fig. 1 (A) The set-up for 3D behavior recording placed inside of the tarp-covered photobox showing the wooden frame used to mount the top-facing video camera, the 3D arena in center, with ruler attached for scale, flanked by LED panels on each side, and the front facing video camera. (B) A schematic of the arena set-up showing relative placement of the arena, cameras, and lights. Solid lines indicate seawater volume, while dotted lines indicate arena volume (not to scale, see supplementary Fig. S2). The accompanying model system for the side view (C) and top view (D) to correct positional data for the effect of diminishing axes frames

Fig. 2 The proportion of paralarval time spent in the top depth bin in the 2D arena of Experiment 1 across CO_2 treatments from trials in 2013 (A), 2014 (B), and all trials compiled (C). Dotted circles denote medians and plus signs denote outliers. Lower case letters denote statistical groups

Fig. 3 (A) Vertical swimming profile for an ambient (400 ppm) *D. pealeii* paralarvae (individual 69_69_08_02) showing depth (blue), vertical velocity (red), and vertical acceleration (gray) over the entire 120-second recording period. (B) A ten-second slice of the swimming profile in A, from 20 seconds to 30 seconds in the video, shows the paralarvae made "hop and sink" jets during descent, rapid ascent, and slow ascent. The velocity peaks represent individual vertical jets

Fig. 4 (A) Three-dimensional track of a swimming path for an ambient (400 ppm) *D. pealeii* paralarvae (individual 69_69_08_02). The front of the arena, which the side camera was pointed at, was the right axis face. (B) Three-dimensional polygon of volume transited by the paralarvae during recording. (C) Tortuosity of path traversed by the paralarvae sampled on a sliding frame of one-second path segments. (D) Turning angles along paralarval path, sampled at sequential vectors of one-second path segments

Fig. 5 (A) Three-dimensional velocity averaged in ten-second bins across the 120-second recording period. Each line represents an individual paralarvae, with line color denoting their CO_2 treatment (400 ppm, blue; 1000 ppm, green; 1600 ppm, orange; 2200 ppm, red). The thick lines represent the median values for all individuals compiled per each CO_2 treatment. Although

individual are remarkably variable over their path and overall, the median lines demonstrate both the decrease in velocity at exposures above 400 ppm and the consistency in overall behavior over time in the arena. (B) The time-binned average velocity data (lines denote medians, colors denote CO_2 treatment as in A) reinforces the high variability in the whisker length and number of outliers (represented as plus signs), and shows both consistently higher velocities in the 400 ppm treatment and broadly consistent median values within CO_2 treatments across the recording time

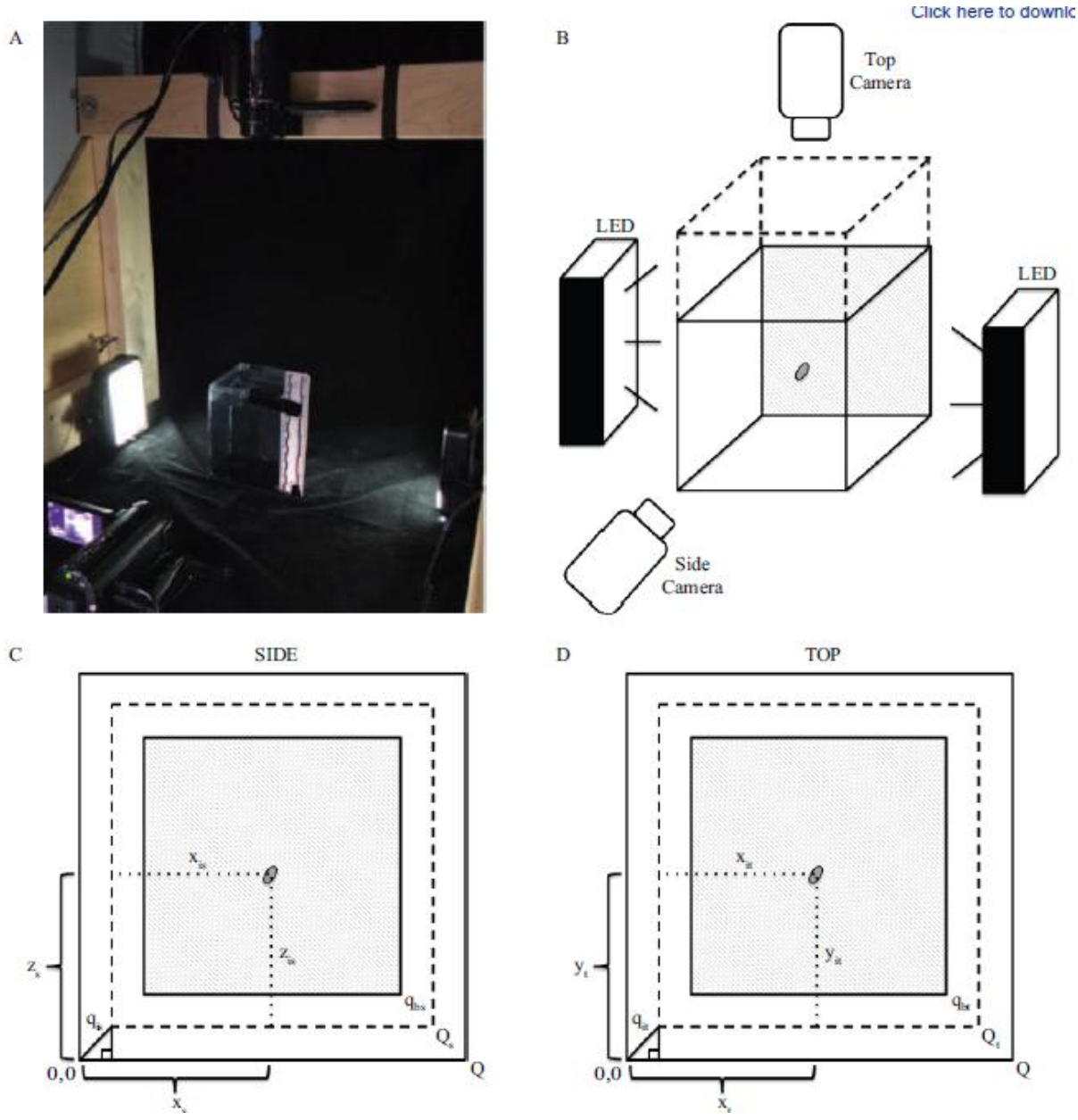

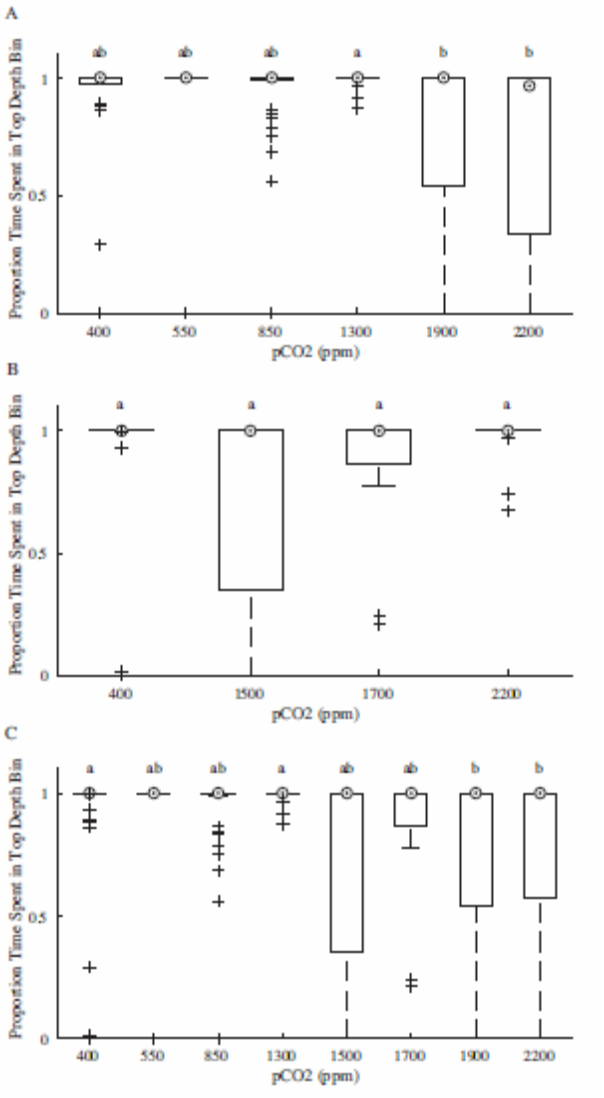
A
ab
ab
ab
a
b
b
Proportion Time Spent in Top Depth Bin
1
0.5
0
400
550
850
1300
1900
2200
pCO2 (ppm)
B
a
a
a
a
Proportion Time Spent in Top Depth Bin
1
0.5
0
400
1500
1700
2200
pCO2 (ppm)
C
a
ab
ab
a
ab
ab
b
b
Proportion Time Spent in Top Depth Bin
1
0.5
0
400
550
850
1300
1500
1700
1900
2200
pCO2 (ppm)

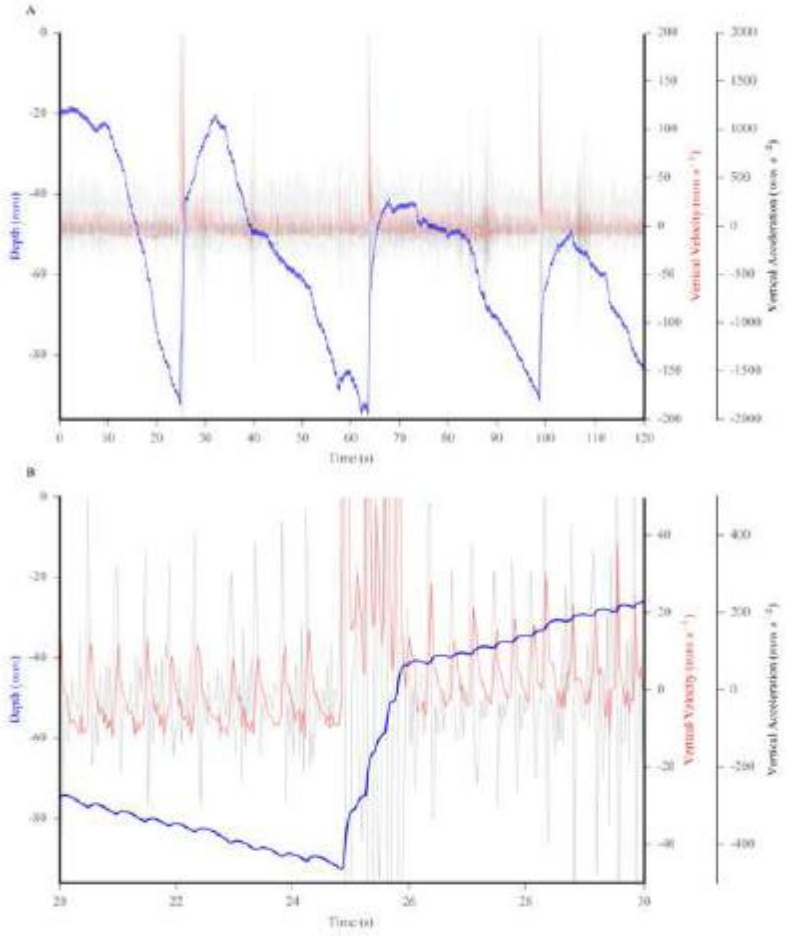
A
B
Time (s)
Time (s)

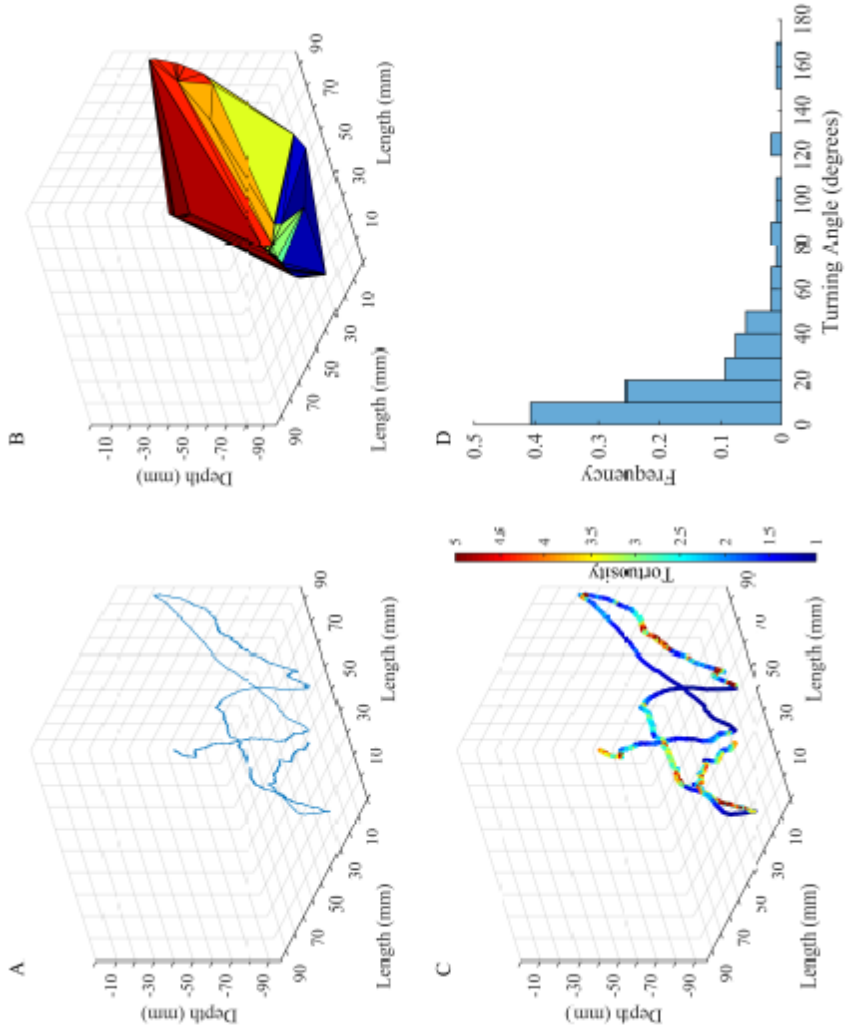
A
B
C
D
Depth (mm)
Length (mm)
Frequency
Turning Angle (degrees)
Tortuosity

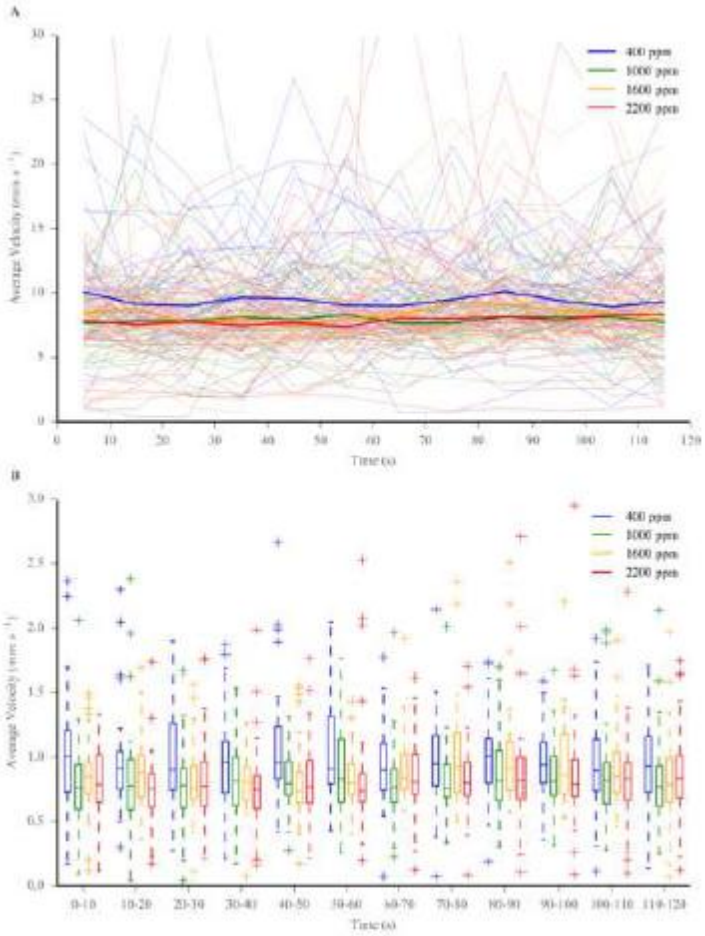
A
400 ppm
1000 ppm
1600 ppm
2200 ppm
Time (s)
B
400 ppm
1000 ppm
1600 ppm
2200 ppm
0-10
10-20
20-30
30-40
40-50
50-60
60-70
70-80
80-90
90-100
100-110
110-120
Time (s)

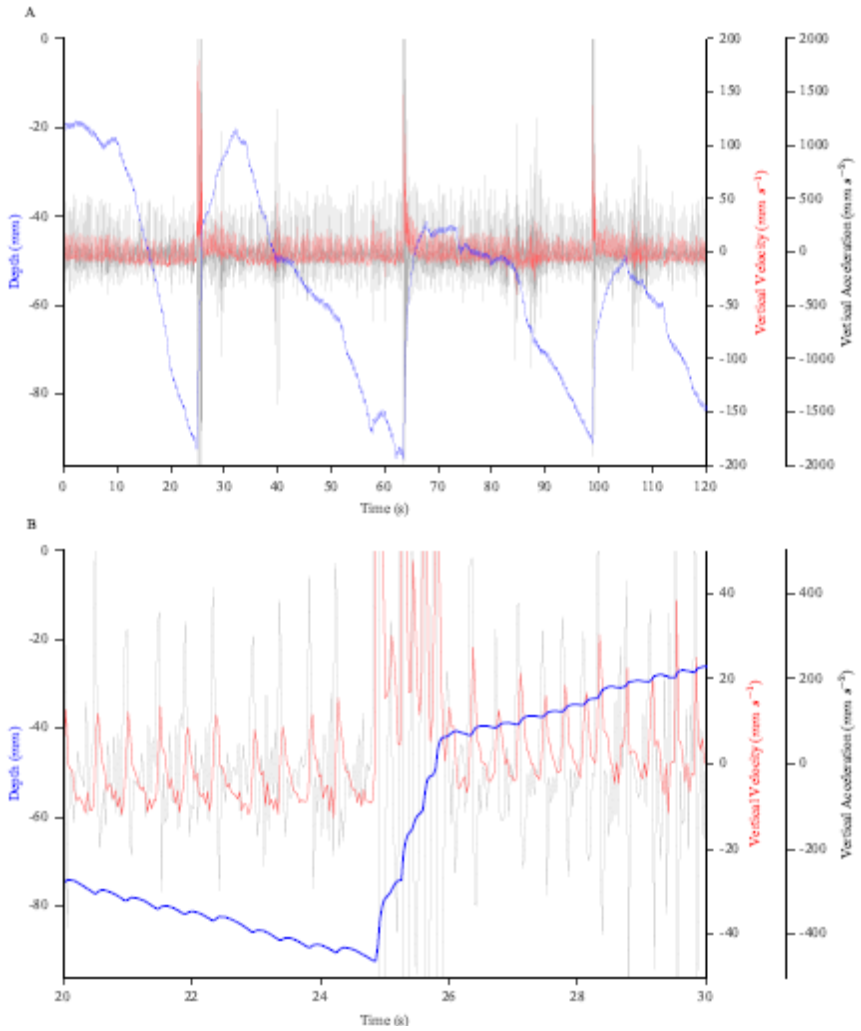
A
Depth (mm)
Vertical Velocity (mm s⁻¹)
Vertical Acceleration (mm s⁻²)
Time (s)
B
Depth (mm)
Vertical Velocity (mm s⁻¹)
Vertical Acceleration (mm s⁻²)
Time (s)

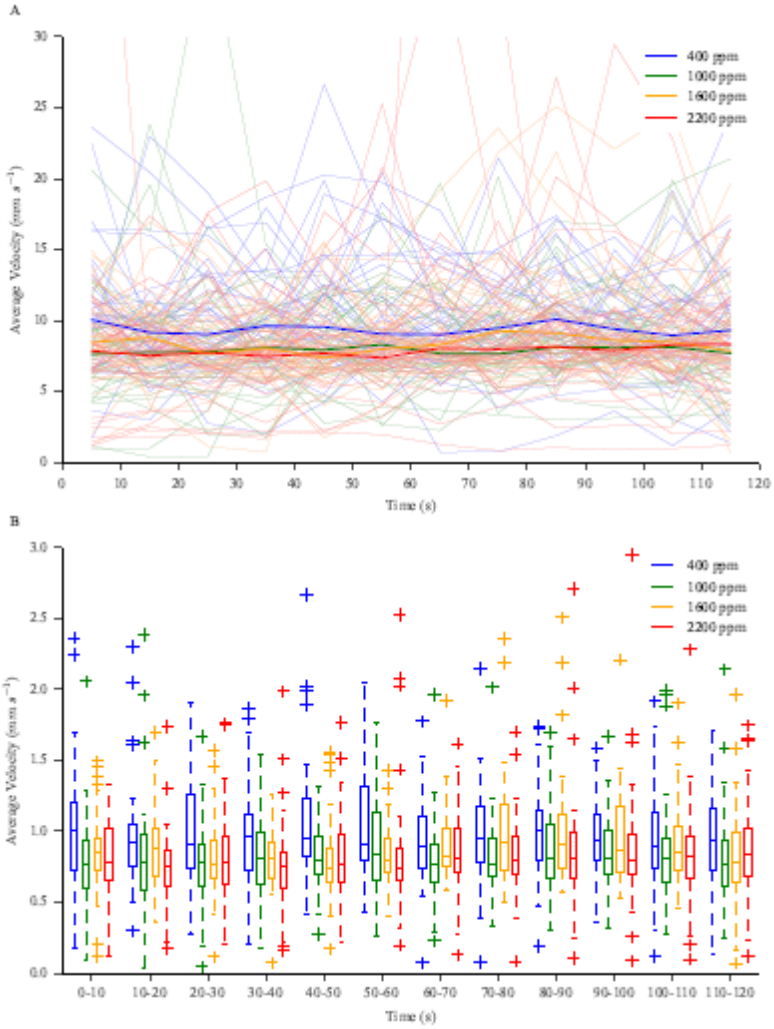

Supplementary Materials

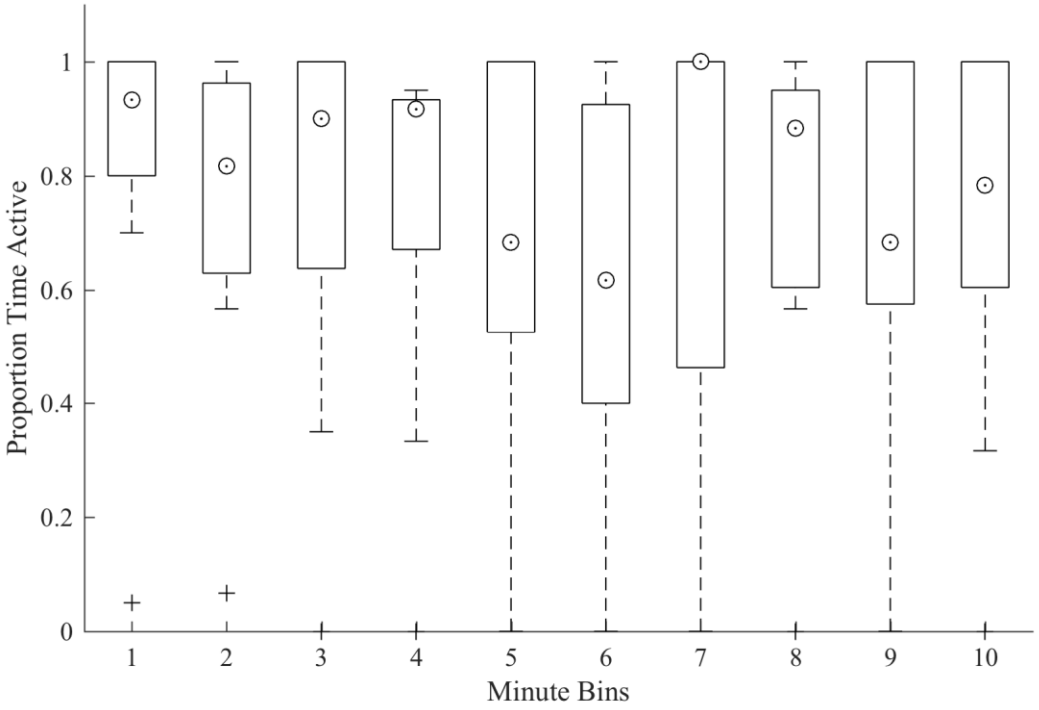

Fig. S1 The proportion of individual paralarval (n = 9) time spent active in one-minute bins over a 10-minute period in the 3D experimental arena. Paralarvae from all 4 CO_2 treatments were used and no consistent pattern with CO_2 exposure was seen, so all data is compiled here. Dotted circles denote medians and plus signs denote outliers

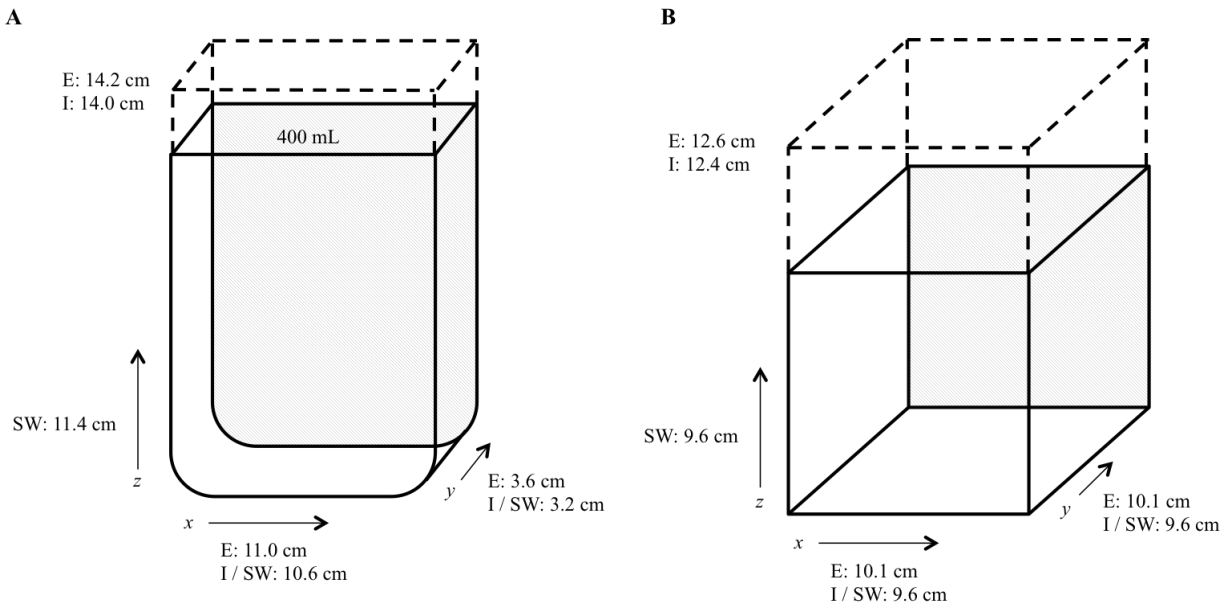

Fig. S2 (A) Dimensions and axes of the 2D arena, constructed from a tissue culture flask. 400 mL of treatment-appropriate seawater was used. (B) Dimensions and axes of the 3D arena constructed from a plastic box. Seawater was added to fill to an internal cube of 9.6 cm. For both schematics, solid lines indicate the seawater space used in the experiments, while dotted lines indicate the additional makeup of the container. Measurements are provided for both external (E) and internal (I) dimensions of the containers, and seawater volume (SW) utilized. The *z* axis is oriented as it was for tracking, in the bottom, front, left (0,0,0) corner. Note that this was transformed, so that 0 was at the water surface, for manuscript figures depicting depth. Figures are not drawn to scale

1. Ocean Acidification and Squid Egg Capsule Culture System

Experiments took place at the WHOI Environmental Systems Laboratory (ESL), Woods Hole, MA from May - October of 2013, 2014, and 2015. A flow-through ocean acidification (OA) system was equilibrated to different CO_2 levels for each trial. Ambient ocean water was pumped in from the ESL intake, passed through the facility's sand-filtration system, and was heated to 20°C. This temperature reflected peak values reached during the breeding season and resulted in a consistent two-week development period for the ambient paralarvae. The seawater was then passed through a 10µm filter (Hayward FLV Series industrial filter equipped with 10µm felt bag) to remove major particulates and a UV sterilizer (Emperor Aquatics Smart HO

UV Sterilizer, Model 025150) to eliminate potentially harmful protozoans. The cleaned water subsequently flowed into the experimental system's header tank and was bubbled with compressed air. Water flowed in a gravity-based system from the header tank and was split among four treatment lines into H-shaped PVC equilibration (EQ) chambers. Each leg of an EQ chamber contained two air stones, which bubbled in the appropriate CO_2 mixture. Due to the elevated CO_2 concentration of ESL seawater (550 ppm in facility compared to 400 ppm at the pump intake in Vineyard Sound) the ambient treatment line was comprised of three EQ chambers, the first degassing with N_2 and the following two reintroducing O_2 and CO_2 at ambient concentrations. Measurements of dissolved oxygen downstream of the nitrogen system were all above 95%. Due to a facility malfunction, Trial 3 of 2013 lost oxygenation downstream of the nitrogen degassing and was not used. To reduce the growth of brown algae, which was encouraged by the nitrogen enrichment, lines were cleaned between each trial and a 1µm filter was placed downstream of the EQ chambers on the ambient line.

Compressed air, delivered at 30 psi from an indoor air compressor, was delivered using a six-way manifold to the header tank aeration, ambient EQ chambers' air stones, and three mass flow controllers (Aalborg GFC17, Orangeburg, NY, USA) with a flow rate of 4.5 l min^{-1}. Pure CO_2 was delivered from a cylinder at 30 psi to three further mass flow controllers (Aalborg GFC17), which were set at various flow rates to produce the desired CO_2 concentrations in the gas mixtures. Air and CO_2 lines were connected downstream of the mass flow controllers and allowed to mix before being split among the EQ chambers' air stones and experimental aquaria bubbling lines. CO_2 mixtures covered a range of values between ambient (400 ppm) and 2200 ppm (Main Text, Table 1). CO_2 concentrations for each level were measured before the start of

each trial on a Qubit Systems CO_2 Analyzer (model s151) calibrated with three commercial reference standards (0, 362, and 1036 ppm).

Equilibrated water in each treatment line outflowed into a PVC manifold and entered drip lines connected to the experimental aquaria, consisting of individual 1-liter PET food service containers (Solo Foodservice, Lake Forest, IL). The containers had been seawater soaked for 24 hours and DI-water rinsed in advance to remove any potential chemical residues or toxins. Cups were sealed with fitted lids pierced with two holes for the gas and equilibrated water lines. Each cup had a small (2x4 cm), screened (5 µm mesh) hole to permit water outflow while retaining paralarvae. The bubbler of the gas line was placed under the screen to create flow and prevent paralarvae from sticking to the screening. Water outflowed from the cups into a common water bath maintained at a temperature of 20°C via aquarium heaters (JÄGER 3603, EHEIM GmbH and Co., Deizisau, DE) and chillers (Oceanic Aquarium Chiller 1/10hp, Oceanic Systems, Walnut Creek, CA, USA).

In 2013, each trial consisted of three CO_2 treatments, each with three experimental cups and one organism-free control cup, totaling twelve cups per water bath. In 2014 and 2015, each trial consisted of four CO_2 treatments, totaling sixteen cups per water bath. The system was run for several days prior to a trial to ensure stable water and gas levels. Flow rates to the cups were set at a slow drip, approximately 20 liters day^{-1}, which prevented waste accumulation. The flow rate also allowed sufficient time for bubbled gas to equilibrate with water in the EQ chambers. The ESL room containing the experimental set up was kept on a 14:10 hour light:dark photoperiod, reflecting the average photoperiod of the region, using ceiling mounted fluorescent lighting. Water bath temperature and ambient light levels were monitored using an Onset HOBO data logger (pendant model UA-004-64), one in each water bath, with recordings taken every 15

minutes. Temperatures were 20.49 ± 0.69 °C, 20.36 ± 1.80 °C, and 20.01 ± 1.00 °C (mean ± SE) in water bath 1 and 20.26 ± 0.49 °C, 20.18 ± 1.74 °C, and 20.51 ± 1.91 °C in water bath 2 in 2013, 2014, and 2015, respectively.

Once squid were brought to the ESL holding tanks, females began laying eggs within two to three days, producing small egg mats typically found at the bottom of the tank or attached to the air hose. The morning an egg cluster was found, it was removed to a holding container and examined for quality. Individual egg capsules, each containing between 50-200 eggs, were then randomly selected and randomly assigned to each experimental cup, with two egg capsules per cup (18 egg capsules per trial for 2013, 24 for 2014 and 2015), marking the start of a trial.

During a trial, pH measurements were taken for samples from each cup every three days using a pH meter (Orion Star™ A329, Thermo Fisher Scientific Inc., Waltham, MA, USA) in order to monitor CO_2 level stability. The fourth cup from each CO_2 level contained no eggs sacs and was used as a control for water quality and carbonate chemistry measurements. Spectrometric pH measurements were taken with a spectrophotometer using methods adapted from Clayton and Byrne (1993) and Dickson et al. (2007) Salinity was measured using a salinity probe (Orion Star™ A329, Thermo Fisher Scientific Inc., Waltham, MA, USA) in parallel to spectrophotometric pH readings. Total alkalinity (AT) samples were taken in 20mL acid-washed, glass scintillation vials and poisoned with 10µL saturated mercuric chloride (HgCl2). Alkalinity samples were analyzed post-trial using an automated small volume titrator (Titrando 808, Metrohm AG, Herisau, CH) programmed to run Gran titrations of 1mL subsamples. Samples were run in duplicate and calibrated against standards of ESL water of known alkalinity. For duplicates with a difference of 4 µmol kg^{-1} seawater (SW) or greater, samples were rerun and an average of the four values was taken. Carbonate chemistry metrics (temperature, salinity, pH,

and alkalinity) were input into CO2SYS, using dissociation constants from Mehrbach (1973) and sulfate constants from Dickson (1990), to calculate pCO_2 and aragonite saturation state (Ω_{arag}) for each treatment of each trial. A baseline measurement of all cups was taken prior to the initiation of a trial, followed by weekly readings of only the control cups once a trial had begun. Measured seawater CO_2 concentrations fell within reasonable range of the equilibrations desired from the gas concentrations (Main Text, Table 1).

2. Recording 3D Swimming Behavior Videos

2.1 3D Swimming Behavior Recording Protocol

1. Before sampling your organism, make sure the setup is complete as follows (Note: all cameras and the organism aquaria/chamber were placed within a covered photography light box to block ambient light):
    a) Fill the chamber with seawater appropriate to the treatment you are testing. The water level needed to make a perfect cube (9.6 cm for this chamber) is marked with a small black line. Remove any bubbles by scraping with a ruler.
    b) Secure the top camera to a sturdy frame above where your chamber will be placed.
    c) Place the chamber beneath the top camera. Adjust the top camera zoom so the entire chamber is clearly visible within the image frame.
    d) Center the chamber in the camera view. This can be done by measuring the distance between the sides of the chamber and the edge of the image frame for each side and making this distance on both sides equal.
    e) Ensure the camera is viewing the center of the chamber straight on and is not skewed to any angle. This can be done by measuring the length (in the camera image) from the top (front) edge of each side of the chamber to its bottom (back) edge and adjusting the position of the camera and chamber to make these distances equal.
    f) Place the side camera on a raised block in front of the chamber, such that the camera points to the center of the chamber. Adjust the zoom so the entire chamber is clearly visible. Center the camera on the chamber and adjust skew, as above. Connect the cameras to viewing monitors outside your light box.
    g) Place one light on either side of the chamber (perpendicular, non-biased lighting is necessary for photopositive organisms only). Set lighting so your organism is clearly visible in both camera images and reflections from your chamber are reduced as much as possible.
2. Select one individual and place it into the center of the chamber.
3. Close the cover of the light box. Allow organism to acclimate to chamber (one minute was suitable for squid paralarvae).
4. Start timer and record for desired length (two minutes was suitable for squid paralarvae).
5. Before stopping the recording, use a light, laser, or other visual cue so that both videos can easily by synced for 3D analysis.
6. Stop the recording. Remove organism. Repeat steps 3-7 for as many individuals as you have per treatment.
7. Record file number for top and side camera and relevant experimental data/individual identification on a data sheet, along with any notes on video quality (good swimming, corner, etc).

8. Note: Remember to change water in filming chamber as needed as you progress through your treatments. The camera adjustments outlined in step 1 must be repeated/checked each time the organism chamber is removed or replaced.
9. Upload video files to an external hard drive (recommended due to size and number of videos). Save files in a dated folder, and within that, either a "top" or "side" subfolder.
10. Double check to ensure your recordings are saved and backed up before reformatting the memory cards for the next recording session.

3. Analysis of 3D Swimming Behavior Data

3.1 Organism Tracking Protocol

1. Drag your video into Tracker (available at OpenSourcePhysics.org). It is best to analyze videos one minute at a time because Tracker can slow down and can run out of memory (amount of memory available to Tracker can be adjusted by clicking **memory in use →Set memory size…**). Save as you go. If the memory allotment gets overloaded the program can crash. At a higher memory allotment, a full two-minute video can be analyzed in one Tracker run. In order to clear the memory cache, it is easiest to close and reopen Tracker for each video analyzed.
2. In the top right corner, click the "refresh" button then deselect **Auto-refresh**. This prevents available memory from filling up as you track, which slows down the process.
3. You may need to correct for stretching due to Tracker's pixel size, which may differ from those used your camera. Click **Video →Filters →New →Resize**, then adjust. For the Sony HD Handycams used in the squid experiment the adjustment was:

	Width	Height
Input	**1440**	**1080**
Output	**1440**	**800**

4. Adjust the axis to the desired position by clicking the magenta axis button (**show or hide the coordinate axes)** on the tool bar. From the side view, the origin (0,0) point should be in the top left corner of the chamber with the y-axis aligned with the inside of the left edge of the chamber and the x-axis aligned with the water level. You can tilt the axes, if needed, by clicking and dragging them. The axes for the top view depend on how your camera is oriented in relation to chamber. The origin for all the data should be the top, left, front corner of the chamber. Our top camera was placed such that it viewed the chamber with the front edge at the top of the image. Thus, we placed the origin for tracking top videos at the top right corner of the chamber with the y-axis aligned with the inside right edge of the chamber and the x-axis aligned with the inside top edge. This produced negative values for both x and y data that had to be later reoriented (multiply by -1) to the correct reference frame.
5. Adjust the scale by pressing the blue **Show, hide, or create calibration tools** on the toolbar. Click on **new →alibration tape.** A blue, double-headed arrow will appear on screen. Drag the ends of the calibration tape across a known distance, typically the length of your chamber (9.6 cm between the inside edges of the chamber). You can zoom in to be as accurate as possible placing the ends of the tape. Make sure the angle of the tape to the x-axis is 0. Double click on the box with the blue number and change it to your known length (9.6 in our case) once adjusted perfectly.
6. Frame selection:
    a. Calculate the total number of frames analyzed for 1 minute of video. For our cameras this was 1799, since the camera filmed at 29.97 frames per second.
    b. To calculate the frames you would like to analyze, find the frame where the laser pointer first appears signaling the end of the recording and use the frame before as the last. Subtract your desired number of frames -1 (1798, in our case) from the last frame to get the first frame (the frame range is inclusive, hence we subtracted 1798 not 1799).

7. To apply the desired frame range, click on the **Clip Settings** button on the toolbar. Enter the frame numbers in the window that appears. You can tell the range has been applied because the small black arrows beneath the video scanning bar at the bottom of the screen will have moved to enclose the desired range.
8. To start a new track, click **Create a new track →Point Mass.** Click on the **mass a** button in the Track Control window and click the **Autotracker…** button, which will open the Autotracker window.
9. Autotracker: (refer to **Help →Tracker Help →Autotracker** for further explanation)
    a. Autotracker works best when the organism is a well-lit white dot and against a black background.
    b. To start, **shift + control + click** on the animal to be tracked. The numbered point is the **target**; its position is what will be marked in the data column. The circle selects the **template image** autotracker will search for, it will appear in the autotracker window. It can be manually resized and moved in relation to the **target**, but the target will stay wherever you have placed it in relation to the **template image** while tracking (should be inside the circle).
    c. The dashed rectangle is the **search area**, in which autotracker will search for the **template image** in the next frame. Depending on how fast/far per frame the animal is moving, make this as small as possible.
    d. Press the **search** button for autotracker to automatically check each frame for the image.
    e. Watch Autotracker for the entire time! If it is no longer following the animal, push the stop button and backtrack to the frame where the **target** lost the animal.
    f. To create a new template image, delete the current point and **shift + control + click** on the animal again to create a new **key frame**. If you do this without deleting the current point you will just create a new template image, the **target** will not be moved and will place data points incorrectly. Always make sure the target is not placing data points outside the template image.
    g. You can also try dragging the **search area** box back over the organism and then clicking **search.**
    h. If tracker is having a hard time, you can manually track by repeatedly using **shift + click** to place the target on the animal frame-by-frame until autotracker can be used again.
    i. Use the **evolution rate** to tell autotracker how much the template image will change frame-to-frame; usually it can be lower than default. Use the **automark** to set the minimum match score needed to mark points. Lower numbers result in more false-matches but fewer stoppages.
10. Autotracker data:
    a. Adjust the **frame range** in **Clip Settings** to include the entire tracked time, including first and last frames. Select your point mass (usually mass A) from the Plot or Table dropdown menu, and then click the **Refresh data and views** button on the right side of the toolbar.
    b. Copy and paste the table data into an Excel document.
    c. Autotracker occasionally skips frames, so it is necessary to check for missing data points. In Excel, select all the data and then use the **Go To** function (Fn+F5 on PC), then click **Special** and check **Blanks**. This highlights all blank cells. You can then change fill color to red to be more visible, and then scroll through to find missing data. Then, go back into the Tracker file and find the skipped frame, **shift-click** to manually mark the position of the organism and copy the needed data back into Excel.
11. Save the tracker file and the Excel file of your data.
12. In Tracker, use a calibration tape (**Show, hide, or create calibration tools →new →calibration tape**) to measure the length of the back of the chamber for q_{bs} or q_{bl} (See list of model variables below). These values are the same throughout a certain placement and orientation of the cameras and chamber, so only need to be measured once for each block of recording (i.e. if the cameras or chamber get moved/readjusted, then measure these values again).

3.2 3D Data Analysis Protocol

1. Compile the side and top data for each individual into a single Excel file with the columns: time (s), xs, zs, xt, yt (time can be converted to seconds from frame number, xs and zs are the x and y data from the side view while xt an yt are the x and y data from the top view, respectively). Ensure that your data is oriented to an origin (0,0,0) at the top, left, front corner of the chamber (particularly your top view data).
2. Open Matlab and run the *Behavior3DCorrection* code (below). Enter your Excel file name, sheet name, data range, q_{bs} and q_{bt} for the video you are analyzing. The code usually takes several minutes (5 - 10) to run for two minutes of data. This code outputs your corrected time, x, y, z position data in a new .xls or .csv file and automatically calls *Behavior3DAnalysis* to calculate metrics of movement.
3. *Behavior3DAnalysis* calculates a number of 3D movement metrics and prints the summary results of this data to a results text file as well as full data to individual .xls or .csv files. It also produces several preliminary plots of the individual organism's movement to aid in visualization and further analysis.

3.3 List of Model Variables

List of Model Variables

q_{bs}	length of back plane of chamber in side video image
q_{bt}	length of back plane of chamber in top video image
q_{is}	hypotenuse formed between front plane and side view image plane
q_{it}	hypotenuse formed between front plane and top view image plane
Q	length of cubic chamber side
Q_s	length of image plane of organism in side view
Q_t	length of image plane of organism in top view
x	true x position of organism
x_{is}	x position in side view image plane
x_{it}	x position in top view image plane
x_s	measured x position in side view tracking
x_t	measured x position in top view tracking
y	true y position of organism
y_{it}	y position in organism's top view image plane
y_t	measured y position in top view tracking
z	true z position of organism
z_{is}	z position in side view image plane
z_s	measured z position in side view tracking

3.4 3D Behavior Data Correction MATLAB code

```
function Behavior3DCorrection
%{Behavior3DCorrection is designed to merge and correct x,z (side view) and
%x,y (top view) tracking data derived from video of an organism (a squid
%paralarvae) swimming in a cubic arena taken with two perpendicular cameras.
%This code assumes the data is stored in a single Excel spreadsheet where
%the columns are: time (s), xs, zs, xt, yt. These known data are input into
%an overconstrained system of equations and assessed using least sum of
%squares to approximate the true x, y, and z values with the most minimal
%error. This code accompanies the publication: Zakroff, C. Mooney, TA,
%Wirth, C. Ocean Acidification Responses in Paralarval Squid Swimming
%Behavior Using a Novel 3D Tracking System. (2017). Hydrobiologia Vol: Pages.
%DOI:
%
%Version 1.5 written by Casey Zakroff (czakroff@whoi.edu) May 11 2017
%in MATLAB version 2016b on Mac. Code and protocols available at:
```

```
%https://github.com/czakroff/3D-Swimming-Behavior
%}

%User Input of Excel Data Sheet
filename = input('\nEnter the name of the Excel file: ', 's');
sheet = input('Enter the name of the Excel sheet: ', 's');
dataRange = input('Enter the range of the data cells, i.e. "A5:E3602":', 's');
%This data range works for 2 minute videos (3598 frames)
pLcode = strcat(filename,'_',sheet); %ID code for each individual squid
paralarvae (pL)

%Read in t, xs, zs, xt, yt
rawData = xlsread(filename, sheet, dataRange);

%Establish known values of from your arena
Q = 9.6; %Q is the length of the side of your cubic arena (in cm)
%Read in Qbs - the length of the back of the arena in the side video image
Qbs = input('Enter Qbs value: ');
%Read in Qbt - the length of the back of the arena in the top video image
Qbt = input('Enter Qbt value: ');

%Calculate the hypoteneuse of the right triangle between Q and Q back for both
the side and top.
qbs = (Q-Qbs)/2*sqrt(2);
qbt = (Q-Qbt)/2*sqrt(2);

%Set up output data array and assign time to first column
correctedData = zeros(size(rawData,1),4);
correctedData(:,1) = rawData(:,1);

%Assign xs, zs, xt, and yt
xs = rawData(1:size(rawData,1),2);
zs = rawData(1:size(rawData,1),3);
xt = rawData(1:size(rawData,1),4);
yt = rawData(1:size(rawData,1),5);

%Assign limits and options for fmincon
A = ones(1,11)*0.001;
B = ones(1,11)*Q;
options = optimoptions('fmincon','Display','final');

for i = 1:size(rawData,1)
    %Assign guesses for fmincon
    % x0 = [x, y, z, xis, zis, xit, yit, qis, qit, Qs, Qt]
    x0 = [xs(i), yt(i), zs(i), xs(i), zs(i), xt(i), yt(i), 0, 0, Q, Q];

    %Run least sum of squares using fmincon
    [p,fval,exitflag,output] =
fmincon(@leastSumSqr,x0,[],[],[],[],A,B,[],options);
    correctedData(i,2:4) = p(1:3); %store corrected t,x,y,z data
end

%Output corrected data. Creates CSV on Macs
xlswrite(pLcode, correctedData);

%Call analysis code to get 3D metrics and basic plots
Behavior3DAnalysis(correctedData,pLcode);

%System of equations assessed by fmincon
```

```
    function fVal = leastSumSqr(x0)

        F = zeros(1,12);

        F(1) = x0(1)*x0(10)/x0(4)-Q;
        F(2) = x0(3)*x0(10)/x0(5)-Q;
        F(3) = x0(1)*x0(11)/x0(6)-Q;
        F(4) = x0(2)*x0(11)/x0(7)-Q;
        F(5) = (x0(4)+x0(8)/sqrt(2))-xs(i);
        F(6) = (x0(5)+x0(8)/sqrt(2))-zs(i);
        F(7) = (x0(6)+x0(9)/sqrt(2))-xt(i);
        F(8) = (x0(7)+x0(9)/sqrt(2))-yt(i);
        F(9) = (x0(10)+2*x0(8)/sqrt(2))-Q;
        F(10) = (x0(11)+2*x0(9)/sqrt(2))-Q;
        F(11) = x0(8)/x0(2)-qbs/Q;
        F(12) = x0(9)/x0(3)-qbt/Q;

        fVal = sum(F.^2);
    end

end
```

3.5 3D Behavior Analysis MATLAB code

```
function Behavior3DAnalysis(data, filename)
%{Behavior3DAnalysis takes the corrected x, y, z positional data from
%Behavior3DCorrection and calculates total distance traveled, average,
%peak, min, max, and median of 3D, horizontal, and vertical velocity, 3D
%volume covered, 2D turning angles, and path tortuosity (a ratio of the
%distance transitited between two points and the true distance between those
%points) of an individual swimming organism. These data are output to a
%'results' text file and to an Excel file named with the individual
%organism ID code. A 3D plot of the organism's swimming track, a plot of
%the tortuosity of that path, and a 3D polygon of the volume covered by the
%organism are produced and output as tiff files. A histogram of the
%organism's turning angles over the entire track is output as a png.
%This code accompanies the publication: Zakroff, C. Mooney, TA,
%Wirth, C. Ocean Acidification Responses in Paralarval Squid Swimming
%Behavior Using a Novel 3D Tracking System. (2017). Hydrobiologia. Vol: Pages.
%DOI:
%
%Version 1.5 written by Casey Zakroff (czakroff@whoi.edu) May 11 2017
%in MATLAB version 2016b on Mac. Code and protocols available at:
%https://github.com/czakroff/3D-Swimming-Behavior
%}

%Set variables to set sampling resolution for tortuosity and turning angle
res = 30; %Sampling resolution (value is in frames; 30 fps = 1 s segments)
numPts = floor(size(data,1)/res); %Number of points sampled from the data

%Create arrays to store 3D metrics
distance = zeros(size(data,1)-1,1);
vel = zeros(size(data,1)-1,1); %3D velocity
vertVel = zeros(size(data,1)-1,1); %vertical velocity
horVel = zeros(size(data,1)-1,1); %horizontal velocity
angles = zeros(numPts-1,1); %turning angles
tort = zeros(size(data,1)-res-1,1); %tortuosity
```

```
%Calculate total distance traveled (cm) and velocities (cm/s)
%by looping through all data and recording values between successive
%positions.
for i = 1:(size(data,1)-1)
    tDiff = data(i+1,1)-data((i),1); %difference in time (s)
    xDiff = data(i+1,2)-data((i),2); %difference in x (cm)
    yDiff = data(i+1,3)-data((i),3); %difference in y (cm)
    zDiff = data(i+1,4)-data((i),4); %difference in z (cm)
    distance(i) = sqrt(xDiff^2+yDiff^2+zDiff^2);
    vel(i) = distance(i)/tDiff;
    vertVel(i) = zDiff/tDiff;
    horVel(i) = sqrt(xDiff^2+yDiff^2)/tDiff;
end

%Store distance and speed data
totDist = sum(distance);
avgVel = mean(vel);
peakVel = max(vel);
minVel = min(vel);
medVel = median(vel);
avgVVel = mean(vertVel);
peakVVel = max(vertVel);
minVVel = min(vertVel);
medVVel = median(vertVel);
avgHVel = mean(horVel);
peakHVel = max(horVel);
minHVel = min(horVel);
medHVel = median(horVel);

%Calculate hull (for polygon) and 3D volume covered
[K,vol3D] = convhull(data(:,2),data(:,3),data(:,4));

%Calculate 2D turning angles between successive 1-second steps (res)
j = 1;
for i = 1:(numPts-1)
    xdiff1 = data((j+res),2)-data(j,2);
    ydiff1 = data((j+res),3)-data(j,3);
    xdiff2 = data((j+2*res),2)-data((j+res),2);
    ydiff2 = data((j+2*res),3)-data((j+res),3);
    a = [xdiff1,ydiff1];
    b = [xdiff2,ydiff2];
    angle = atan2(abs(det([a;b])),dot(a,b));
    angles(i) = angle*180/pi;
    j = j+res;
end

%Store turning angle data
avgAngl = mean(angles);
maxAngl = max(angles);
minAngl = min(angles);
medAngl = median(angles);

%Tortuosity
%Loop for calculating tortuosity over 1-second steps (res)
for i = 1:(size(data,1)-res-1)
    xDiffT = data((i+res),2)-data((i),2);
    yDiffT = data((i+res),3)-data((i),3);
    zDiffT = data((i+res),4)-data((i),4);
    distPts = sqrt(xDiffT^2+yDiffT^2+zDiffT^2); %distance between points
    distTort = sum(distance(i:(i+res))); %distance covered by organism
```

```
    tort(i) = distTort/distPts;
end

%Store tortuosity data
avgTort = mean(tort);
peakTort = max(tort);
minTort = min(tort);
medTort = median(tort);

figure
fig = gcf;
fig.PaperUnits = 'centimeters';
fig.PaperPositionMode = 'manual';
fig.PaperSize = [33.8 33.8];

%Plot 3D track and output tiff
plot3(data(:,2),data(:,3),data(:,4)-9.6);
ax = gca;
ax.FontUnits = 'centimeters';
ax.FontName = 'Times New Roman';
ax.FontSize = 0.35;
ax.XTickMode = 'manual';
ax.YTickMode = 'manual';
ax.XLimMode = 'manual';
ax.YLimMode = 'manual';
ax.XLim = [0,9.600];
ax.YLim = [0,9.600];
ax.ZLim = [-9.600,0];
ax.XTick = [0,1,2,3,4,5,6,7,8,9];
ax.XTickLabel = {' ', '1', ' ', '3', ' ', '5', ' ', '7', ' ', '9'};
ax.YTick = [0,1,2,3,4,5,6,7,8,9];
ax.YTickLabel = {' ', '1', ' ', '3', ' ', '5', ' ', '7', ' ', '9'};
ax.ZTick = [-9,-8,-7,-6,-5,-4,-3,-2,-1,0];
ax.ZTickLabel = {'-9', '', '-7', '', '-5', '', '-3', '', '-1', ''};
ax.XGrid = 'on';
ax.YGrid = 'on';
ax.ZGrid = 'on';
ax.XLabel.String = 'Length (cm)';
ax.YLabel.String = 'Length (cm)';
ax.ZLabel.String = 'Depth (cm)';
print('-dtiff','-r600',filename);

%Calculate colormap for tortuosity plot
[t1,t2] = size(tort);
[d1,d2] = size(data(:,2));
col = tort;
for i = t1:d1-1
    col = [col; tort(t1)];
end

%Plot tortuosity as thin 3D surface and output tiff
h = surface([data(:,2), data(:,2)], [data(:,3), data(:,3)],...
    [data(:,4)-9.6, data(:,4)-9.6],[col,col],...
    'FaceColor','none','EdgeColor','interp','LineWidth',2);
colormap(jet);
caxis([1 5]);
c = colorbar;
text('String','Tortuosity', 'Rotation', 90,...
    'Position', [242.25 302.5 -227.2],...
    'FontUnits', 'centimeters', 'FontSize', 0.35,...
```

```
    'FontName', 'Times New Roman', 'color','k');
print('-dtiff','-r400',strcat(filename,'_tortuosity'));

%Create 3D volume polygon and output tiff
colormap(parula);
trisurf(K,data(:,2),data(:,3),data(:,4)-9.6);
ax = gca;
ax.FontUnits = 'centimeters';
ax.FontName = 'Times New Roman';
ax.FontSize = 0.35;
ax.XTickMode = 'manual';
ax.YTickMode = 'manual';
ax.XLimMode = 'manual';
ax.YLimMode = 'manual';
ax.XLim = [0,9.600];
ax.YLim = [0,9.600];
ax.ZLim = [-9.600,0];
ax.XTick = [0,1,2,3,4,5,6,7,8,9];
ax.XTickLabel = {' ', '1', ' ', '3', ' ', '5', ' ', '7', ' ', '9'};
ax.YTick = [0,1,2,3,4,5,6,7,8,9];
ax.YTickLabel = {' ', '1', ' ', '3', ' ', '5', ' ', '7', ' ', '9'};
ax.ZTick = [-9,-8,-7,-6,-5,-4,-3,-2,-1,0];
ax.ZTickLabel = {'-9', '', '-7', '', '-5', '', '-3', '', '-1', ''};
ax.XGrid = 'on';
ax.YGrid = 'on';
ax.ZGrid = 'on';
ax.XLabel.String = 'Length (cm)';
ax.YLabel.String = 'Length (cm)';
ax.ZLabel.String = 'Depth (cm)';
print('-dtiff','-r600',strcat(filename,'_volume'));

%Plot histogram of turning angles and output png
angBins = 18; %Number of bins for angle histogram
histogram(angles,angBins,'BinWidth', 10,'Normalization','probability');
ax = gca;
ax.XTickMode = 'manual';
ax.XLimMode = 'manual';
ax.FontUnits = 'centimeters';
ax.FontName = 'Times New Roman';
ax.FontSize = 0.35;
ax.Box = 'Off';
ax.XLabel.String = 'Turning Angle (degrees)';
ax.XLim = [0 180];
ax.YLim = [0 0.5];
ax.XTick = [0,20,40,60,80,100,120,140,160,180];
ax.YTick = [0,0.1,0.2,0.3,0.4,0.5];
ax.YLabel.String = 'Frequency';
print(strcat(filename,'_turningAngles'), '-dpng');

%Compile results
results = [totDist; avgVel; peakVel; minVel; medVel; avgVVel;
    peakVVel; minVVel; medVVel; avgHVel; peakHVel; minHVel; medHVel;
    vol3D; avgAngl; maxAngl; minAngl; medAngl; avgTort; peakTort; minTort
    medTort];

%Output data to results textfile
fid = fopen('results.txt', 'a');
spec =
'\n\n%s%123.4f%123.4f%123.4f%123.4f%123.4f%123.4f%123.4f%123.4f%123.4f%123.4f%
123.4f%123.4f%123.4f%123.4f%123.4f%123.4f%123.4f%123.4f%123.4f%123.4f%123.4f%1
```

```
23.4f';
fprintf(fid, spec, filename, results);
fclose(fid);

%{
%Output data on PC (output as one Excel file)
xlswrite(filename,results,'results');
xlswrite(filename,distance, 'distance');
xlswrite(filename,vel,'3Dvelocity');
xlswrite(filename,vertVel,'verticalVelocity');
xlswrite(filename,horVel,'horizontalVelocity');
xlswrite(filename,angles, 'angles');
xlswrite(filename,tort, 'tortuosity');
%}

%Output data on Mac (output as individual CSVs)
xlswrite(strcat(filename,'_results'),results);
xlswrite(strcat(filename,'_distance'),distance);
xlswrite(strcat(filename,'_3Dvelocity'),vel);
xlswrite(strcat(filename,'_verticalVelocity'),vertVel);
xlswrite(strcat(filename,'_horizontalVelocity'),horVel);
xlswrite(strcat(filename,'_angles'),angles);
xlswrite(strcat(filename,'_tortuosity'),tort);

end
```

4. References

Clayton TD, Byrne RH (1993) Spectrophotometric seawater pH measurements : total hydrogen results. Deep Res 40:2115–2129

Dickson AG (1990) Standard potential of the reaction: , and and the standard acidity constant of the ion HSO4− in synthetic sea water from 273.15 to 318.15 K. J Chem Thermodyn 22:113–127

Dickson AG, Sabine CL, Christian JR (2007) Guide to best practices for ocean CO2 measurements. PICES Spec Publ 3:p191

Mehrbach C, Culberson CH, Hawley JE, Pytkowicz RM (1973) Measurement of the apparent dissociation constants of carbonic acid in seawater at atmospheric pressure. Limnol Oceanogr 18:897–907